Transient Seakeeping Analysis Using Generalized Modes

by

Thomas Henning Farstad

Candidatus Magesterii, University of Oslo, 1995

Submitted to the Department of Ocean Engineering
in partial fulfillment of the requirements for the degree of

Master of Science in Naval Architecture and Marine Engineering

at the

MASSACHUSETTS INSTITUTE OF TECHNOLOGY

February 1997

Author .....
Department of Ocean Engineering
December 12, 1996

Certified by .....
F. Thomas Korsmeyer
Research Engineer, Research Laboratory of Electronics
Thesis Supervisor

Accepted by .....
J. Kim Vandiver
Chairman, Departmental Committee on Graduate Students

Transient Seakeeping Analysis Using Generalized Modes

by

Thomas Henning Farstad

Submitted to the Department of Ocean Engineering
on December 12, 1996, in partial fulfillment of the
requirements for the degree of
Master of Science in Naval Architecture and Marine Engineering

Abstract

Linear seakeeping theory is reviewed and extended from 6 degrees of freedom to N degrees of freedom, so that hydroelastic problems and multibody problems can be solved in the time-domain. The general form of the 'm-terms' is derived for an arbitrary modeshape, and the problem is solved in 3D using a free-surface Green function and planar, constant-strength panels. Emphasis is on applying the theory of generalized modes in simple problems involving fluid-structure interaction and mulitbody interaction. The generalized modes are also used to obtain an efficient expansion of the load-distribution on a structure when the structure is assumed stiff. This allows for an easy calculation of the bending moments and shear forces in the structure. Good agreement is found with experiments for the Wigley hull.

Thesis Supervisor: F. Thomas Korsmeyer
Title: Research Engineer, Research Laboratory of Electronics

Acknowledgments

I wish to express gratitude to all members of the Computational Hydrodynamics Facility at the Department of Ocean Engineering. In particular to my academic advisor Professor J. N. Newman and my thesis advisor Dr. F. T. Korsmeyer. Together with Dr. C.-H. Lee they gave invaluable guidance throughout my time at the Institute, and they always provided incentive and encouragement to carry on when things did not look so bright.

Three people were indeed of importance in the preparation for MIT. The contributions from Professor J. Grue and Associate Professor H. P. Langtangen at the University of Oslo and my friend, Principal T. Slyngstadli of Vatne Ungdomsskule were crucial in my preparations. Without their help I could never have attended MIT.

Funding was received through a fellowship provided by the Department of Ocean Engineering, a scholarship from The John D. Archbold Fund through The Norway-America Association and Nansen Fund Inc., a scholarship from The Haakon Styri Fund through The American-Scandinavian Foundation, and from Lise and Arnfinn Hejes Fond. All contributions are deeply appreciated.

The work was done in conjunction with the Joint Industry Project "Wave effects on Offshore Structures".

I dedicate this work to my grandparents, Marie and Peder Årvik and Valborg and Aslak Farstad.

Contents

List of Figures

List of Tables

Chapter 1

Introduction

Over the past decades, numerical studies of seakeeping problems have made a giant leap forward. Mostly this is due to the computer power available for a reasonable price. Formulating the seakeeping problem mathematically gives rise to large systems of equations, which can be solved only by the use of computational power. With the introduction of the digital computer in the 1950's, researchers were able to pursue the seakeeping problem with a new and powerful tool. First by using two-dimensional strip theory solving the linearized problem, later using three dimensional theory, both linearized and non-linear formulations.

The fully non-linear problem is still too large to solve, but partly non-linear problems have been studied, for instance by Lin et al. [16] and by Kring et al. [14]. They satisfy the boundary condition on the body surface exactly, but the free surface condition is modified. Kring et al. are using the weak-scatter hypothesis, whereas Lin et al. are linearizing the free surface condition about the undisturbed incoming wave profile. The linear problem is well documented in Bingham et al. [3], and Korsmeyer and Bingham [11]. The general theory for the linear seakeeping problem was given by Newman [21].

In seakeeping, one only considers the six degrees of freedom for a floating body. The behavior of the ship in the presence of waves is of interest in the design and optimization of hull forms, and for extreme value statistics with respect to loads, green water etc. Most of the existing codes for seakeeping analysis are so-called panel

methods. Sources and dipoles are distributed over the body surface (and sometimes over the free surface) and represent the flow in the problem. The force of interest is found from pressure integration. Recently, this has been done in the time domain, earlier only frequency domain quantities were available.

Recent progress in the frequency domain has been to study the wave-structure interaction problem, where the structure is allowed to move and be deformed at the same time. This science is known as hydroelasticity. A practical example is the idea of a floating airport, which from the hydrodynamic point of view has been given a lot of attention lately [23]. The dimension of such a structure will be large compared to the wavelength, and the interaction between the structure and the waves will be of great importance in calculations of the loads. However, all bodies will deform when subject to non-uniform loading like hydrodynamic forces, so the theory of hydroelasticity applies to all bodies which are affected by waves. In the linear problem this will lead to new radiation and diffraction modes. The problem was first formulated by Bishop and Price in [5], Bishop et al. gave later the general theory for hydroelastic structures moving in a seaway in [6]. Newman [19] studied this problem for zero speed, and recent studies have also been performed by Kashiwagi [10] and Wu et al. [29] for large floating structures. Wu et al. have studied the hydroelastic behavior of high speed vessels in [30].

Another group of problems of great interest is the interaction problem which involves several bodies. This problem is very different from hydroelasticity, physically speaking, but the two sets of problems are closely related mathematically. It is therefore possible to develop a theory that is able to handle both hydroelastic problems and interaction problems. Newman studied an array of cylinders in [19], this work was later extended by Maniar et al. [17] to study very large arrays of cylinders. This study was done partly with a general N body theory and partly with the theory of generalized modes. The distinction is the way of attacking the problem. In the N body problem one states explicitly that the problem has N bodies with 6 degrees of freedom if freely floating, if the problem is to be solved in the context of generalized modes, one merely states that this is a wave body interaction problem involving K de-

grees of freedom. If the problem involves N freely floating bodies and no constraints, then K = 6N. Interaction problems are of great importance for offshore operations and for studies of tow problems, for instance. It can also be used in problems involving wall effects. If we consider a ship traveling close to a wall with spacing d, we can represent the wall by using an image of the ship spaced from the original ship with distance $2d$. This way we have two bodies, and the problem can be solved using generalized modes.

In this thesis, the theory of hydroelasticity and seakeeping theory for interaction problems are united in a linear theory that handles both problems in the time domain. Strictly speaking, this is an extension of the traditional seakeeping theory to involve N degrees of freedom for N modes which can be independently chosen. The modes do not have to be rigid. Deformable modes, which will be treated in Chapter 3, can also be used. The problem is formulated as an integral equation, and is solved using a three dimensional low-order panel method. The panels are quadrilateral planar panels, and the potential is assumed constant over the panel. A free-surface Green function, which simplifies the integral formulation to involve integration over the body only, is utilized in order to solve the problem efficiently. Hence, panels need not be distributed on the free-surface and no numerical damping is necessary.

Being able to use generalized modes increases the flexibility of the seakeeping theory. Since all floating bodies will experience wave forces, there will be bending moments and shear forces as a result of the hydrodynamic forcing. Using the generalized modes, we are able to compute these forces within linear theory. It turns out (Section 3.2.1) that the hydrodynamic load distribution can be written down explicitly in terms of the generalized hydrodynamic and hydrostatic quantities. This simplifies the calculations, since there is no need any longer to consider the added mass and damping for a small strip of the hull, for instance.

The method is illustrated through examples dealing with the deformation of a slender barge, which essentially is the same as the floating airport problem. The theory is also applied to a Wigley hull at forward speed, and shear forces and bending moments are calculated using the generalized hydrodynamic quantities. Good

agreement is found with experimental data for the Wigley hull.

Chapter 4 studies the interaction between two hulls at zero and non-zero forward speed. The behavior of the wave in the gap between the two bodies are quite different for these two cases, as will be shown.

The last section contains calculations of steady resistance when two bodies are translating forward in proximity, one ahead of the other. It is shown that the resistance on the aft body is a function of both the separation distance and velocity, and is different from that of a single ship alone.

Chapter 2

Mathematical Formulation

2.1 The Exact Boundary Value Problem

Assuming that the fluid is ideal and the flow irrotational, there will exist a potential Φ such that the velocity in the fluid $\mathbf{V} = \nabla\Phi$, where ∇ is the gradient vector. Conservation of mass requires that $\mathbf{V}$ has zero divergence, hence Φ satisfies Laplace's equation

$$\nabla^2\Phi = 0 \tag{2.1}$$

The pressure p at each point in the fluid is found from Bernoulli's equation

$$p(\mathbf{x_0}, t) = -\rho(\frac{\partial\Phi}{\partial t} + \frac{1}{2}|\nabla\Phi|^2 + gz_0) + p_a \tag{2.2}$$

$\mathbf{x}_0$ is a coordinate system fixed in space, z_0 is the vertical coordinate, measured positive upwards. The pressure on the free surface is p_a and is assumed to be constant. The density of the fluid is ρ and the gravitational acceleration is g. Partial derivation with respect to time is denoted $\frac{\partial}{\partial t}$. The physical understanding of the free surface boundary condition is that a particle on the surface ζ has to remain on the surface. Mathematically this is written

$$\frac{D}{Dt}(z_0 - \zeta) = 0 \tag{2.3}$$

$\frac{D}{Dt} = \frac{\partial}{\partial t} + \mathbf{V} \cdot \nabla$ is the material derivative. This gives the following kinematic free-surface boundary condition:

$$\frac{\partial \zeta}{\partial t} + \frac{\partial \Phi}{\partial x}\frac{\partial \zeta}{\partial x} + \frac{\partial \Phi}{\partial y}\frac{\partial \zeta}{\partial y} = \frac{\partial \Phi}{\partial z} \tag{2.4}$$

The dynamic boundary condition $p = p_a$ takes the form

$$\Phi_t + \frac{1}{2}|\nabla\Phi|^2 + gz_0 = 0 \qquad z_0 = \zeta \tag{2.5}$$

from which we get an explicit formula for the free surface elevation

$$\zeta = -\frac{1}{g}(\Phi_t + \frac{1}{2}|\nabla\Phi|^2) \tag{2.6}$$

Subscripts denote partial differentiation with respect to the variables appearing in the subscripts. Taking the spatial derivative of (2.6) and using (2.4) we get a combined free surface condition

$$g\Phi_z + \Phi_{tt} + 2\nabla\Phi \cdot \nabla\Phi_t + \frac{1}{2}\nabla\Phi \cdot \nabla|\nabla\Phi|^2 = 0 \qquad z_0 = \zeta \tag{2.7}$$

Since (2.7) is second-order in time, we need two initial conditions, which are taken to be

$$\Phi = \Phi_t = 0 \qquad z_0 = 0, t < t_0 \tag{2.8}$$

where t_0 is some arbitrary starting time.

The normal component of the fluid velocity and the body velocity must be equal and opposite on the body boundary.

$$\mathbf{n} \cdot \mathbf{V}_s = \mathbf{n} \cdot \nabla\Phi \qquad \text{on S} \tag{2.9}$$

where $\mathbf{V}_s$ is the ship speed. S is the instantaneous wetted surface of the body. The normal vector $\mathbf{n}$ is taken to point out of the fluid and into the body. This is irrelevant

in (2.9) but will be of importance later. The solution in the far field is specified to be

$$\nabla\Phi \to 0 \qquad |\mathbf{x}| \to \infty \tag{2.10}$$

where all the fluid motion caused by the ship motion will go to zero for all finite times.

2.2 Linearization of the Boundary Value Problem

Assume the amplitude of the motion to be small compared to the wavelength. Derivatives of the potential Φ will then be small, and quadratic terms may be neglected. The free-surface condition (2.7) becomes

$$\Phi_{tt} + g\Phi_z = 0 \qquad z_0 = 0 \tag{2.11}$$

where the free surface ζ also has been expanded around its mean position.

The exact boundary value problem was formulated in an earth-fixed reference frame. This is a suitable choice for the free surface elevation, but less suitable for the flow around a ship hull. For this particular case, a frame of reference fixed to the mean position of a steady translating ship is more suitable. Let ϕ denote the potential in the steady translating frame. The relation between a potential in the two systems is, if the ship speed is $\mathbf{V}_s = U\mathbf{i}$,

$$\Phi(x_0, y_0, z_0, t) = \Phi(x + Ut, y, z, t) = \phi(x, y, z, t) \tag{2.12}$$

The time derivative in the earth-fixed reference frame is a total derivative in the steady translating frame.

$$\Phi_t = \frac{\partial}{\partial t}\phi(x_0 - Ut, y_0, z_0, t) = (\frac{\partial}{\partial t} - U\frac{\partial}{\partial x})\phi(x, y, z, t) \tag{2.13}$$

The free surface condition (2.11) now takes the form

$$(\frac{\partial}{\partial t} - U\frac{\partial}{\partial x})^2\phi + g\phi_z = 0 \qquad z = 0 \tag{2.14}$$

Linearization of the dynamic boundary condition (2.6) gives

$$\zeta = -\frac{1}{g}(\frac{\partial}{\partial t} - U\frac{\partial}{\partial x})\phi \tag{2.15}$$

for the first order wave elevation. Working out the linearized body boundary condition requires some care. Let the potential in the fluid be described by

$$\Phi(\mathbf{x_0}, t) = U\bar{\varphi}(\mathbf{x}) + \varphi(\mathbf{x}, t) \tag{2.16}$$

$\bar{\varphi}$ is the potential due to the steady forward motion of the ship, and φ a pertubation potential, which is assumed to be small [21]. The velocity of the flow relative to the steady moving frame can be described as $\mathbf{W} = U\nabla(\bar{\varphi} - x)$. Let $\bar{S}$ denote the body surface in the steady translating frame. The body boundary condition (2.9) takes the form

$$\mathbf{W} \cdot \mathbf{n} = 0 \qquad \text{on } \bar{\mathrm{S}} \tag{2.17}$$

from which we get the boundary condition for $\bar{\varphi}$

$$\nabla\bar{\varphi} \cdot \mathbf{n} = n_1 \qquad \text{on } \bar{\mathrm{S}} \tag{2.18}$$

Let the ship velocity be described by

$$\mathbf{V}_s = U\mathbf{i} + \dot{\mathbf{a}} \tag{2.19}$$

where $\mathbf{a}$ describes the position of a point of the body in the steady moving reference frame. The over-dot denotes a derivative with respect to time. Using (2.9) we get

$$\varphi_n = \dot{\mathbf{a}} \cdot \mathbf{n} - \mathbf{W} \cdot \mathbf{n} \qquad \text{on S} \tag{2.20}$$

We want to apply this condition on $\bar{S}$, and in order to do so, (2.20) has to be Taylor expanded around $\bar{S}$. It is shown in Appendix A that

$$\mathbf{n}_S \approx \mathbf{n}_{\bar{S}} - \nabla \mathbf{a} \cdot \mathbf{n}_{\bar{S}} \tag{2.21}$$

where tensor notation is used. (2.20) now takes the form

$$\varphi_n \approx [\dot{\mathbf{a}} + (\mathbf{W} \cdot \nabla)\mathbf{a} - (\mathbf{a} \cdot \nabla)\mathbf{W}] \cdot \mathbf{n} \qquad \text{on } \bar{S} \tag{2.22}$$

where (2.17) has been applied. Since all equations now are linearized, the potential φ can be decomposed into

$$\varphi = \varphi_I + \varphi_S + \sum_{k=1}^{K} \varphi_k \tag{2.23}$$

φ_I denotes the incident wave field, the scattered potential is φ_S, a general radiation potential is φ_k and we have a total of K radiation potentials. All potentials will have to satisfy the free surface condition (2.14).

Let

$$\mathbf{a} = \sum_{k=1}^{K} p_k(t)\mathbf{u}_k(x, y, z) \tag{2.24}$$

where $\mathbf{u}_k$ is a vector shape function dependent on the spatial variables with time dependent amplitude or principal coordinate p_k. A rigid-body translation will be represented by a unit vector in that direction, for example $\mathbf{u}_2 = (0, 1, 0)$ represents sway, and $\mathbf{u}_4 = (1, 0, 0) \times \mathbf{x}$ represents roll. A vector $\mathbf{u}_k = (0, 0, \sin qx)$ represents the q-component of a Fourier-sine series describing the deformation in the z-direction. The linearized body boundary conditions for (2.23) can now be expressed as

$$\frac{\partial \varphi_S}{\partial n} = -\frac{\partial \varphi_I}{\partial n} \tag{2.25}$$

$$\mathbf{n} \cdot \nabla \varphi_k = \dot{p}_k n_k + p_k m_k \tag{2.26}$$

where

$$\begin{aligned} n_k &= \mathbf{u}_k \cdot \mathbf{n} = u_{kj} n_j \\ m_k &= -u_{kj}(n_i \tfrac{\partial}{\partial x_i}) W_j + n_j (W_i \tfrac{\partial}{\partial x_i}) u_{kj} \end{aligned} \tag{2.27}$$

The notation is somewhat awkward here, since we are using n_j for both the jth component of the normal vector and the generalized normal vector. It will, however, be relatively easy to understand which is used from the context later in this presentation.

For rigid body mode shapes the m-terms take the form presented in [27], [21].

2.3 Structural Dynamics

This section analyses the behavior of a general structure from a finite element point of view. The analysis is a generalization of the work by Bishop et.al [6].

Consider one single structural element in some discretization of a structure. The displacement of any point within the element (assumed continuous) is specified approximately in terms of a finite number of displacements $\bar{\mathbf{U}}_e$ at the nodes.

$$\bar{\mathbf{u}}(x', y', z') = \mathbf{N}\bar{\mathbf{U}}_e \tag{2.28}$$

where the matrix $\mathbf{N}$ contains suitable shape functions in terms of the local coordinates. The over-bar denotes quantities in the local element frame.

Let $\mathcal{L}$ be some differential operator, then the strain displacement relation $\bar{\epsilon}$ can be written

$$\bar{\epsilon} = \mathcal{L}\mathbf{N}\bar{\mathbf{U}}_e = \mathbf{b}\bar{\mathbf{U}}_e \tag{2.29}$$

where $\mathbf{b} = \mathcal{L}\mathbf{N}$. The stresses are found from Hooke's law

$$\bar{\sigma} = \mathbf{E}\bar{\epsilon} \tag{2.30}$$

where $\mathbf{E}$ contains suitable elastic constants. No thermal effects are considered. The strain energy of the element is given by

$$\Pi_e = \frac{1}{2}\int_{\Omega_e} \bar{\epsilon}^T\bar{\sigma}\, d\Omega \tag{2.31}$$

Ω_e is the volume of the element, and superscript T denotes the transpose of a matrix.

The above expression can be written

$$\Pi_e = \frac{1}{2}\int_{\Omega_e} \bar{\mathbf{U}}_e^T \mathbf{b}^T \mathbf{E}\mathbf{b}\bar{\mathbf{U}}_e \, d\Omega = \frac{1}{2}\bar{\mathbf{U}}_e \bar{\mathbf{K}}_e \bar{\mathbf{U}}_e \tag{2.32}$$

where the stiffness matrix of the element is given as

$$\bar{\mathbf{K}}_e = \int_{\Omega_e} \mathbf{b}^T \mathbf{E}\mathbf{b} \, d\Omega \tag{2.33}$$

The kinetic energy is given by

$$T_e = \frac{1}{2}\int_{\Omega_e} \rho_b \dot{\bar{\mathbf{u}}}^T \dot{\bar{\mathbf{u}}} \, d\Omega = \frac{1}{2}\int_{\Omega_e} \rho_b (\mathbf{N}\dot{\bar{\mathbf{U}}}_e)^T (\mathbf{N}\dot{\bar{\mathbf{U}}}_e) \, d\Omega \tag{2.34}$$

where ρ_b is the density of the material. We can write this

$$T_e = \frac{1}{2}\dot{\bar{\mathbf{U}}}_e^T \bar{\mathbf{M}}_e \dot{\bar{\mathbf{U}}}_e \tag{2.35}$$

where

$$\bar{\mathbf{M}}_e = \int_{\Omega_e} \mathbf{N}^T \rho_b \mathbf{N} \, d\Omega \tag{2.36}$$

The contribution to dissipation can be written as

$$D = \frac{1}{2}\dot{\bar{\mathbf{U}}}_e^T \bar{\mathbf{B}}_e \dot{\bar{\mathbf{U}}}_e \tag{2.37}$$

where $\bar{\mathbf{B}}_e$ is the symmetric damping matrix given by

$$\mathbf{B}_e = \int_{\Omega_e} \mathbf{N}^T \beta \mathbf{N} \, d\Omega \tag{2.38}$$

where β is some specific damping matrix.

External forces acting on the element can be derived from the principal of virtual work. From the fluid pressure p we find

$$\bar{\mathbf{P}}_e = \int_{S_e} p\mathbf{N}^T \bar{\mathbf{n}} \, dS \tag{2.39}$$

where the integration is carried out over the wetted part of the element. The normal vector points out of the fluid and into the element, consistent with the notation in Section 2.2. Other forces acting will be body forces $\mathbf{g}_e$, point forces $\mathbf{F}_e$ and forces from adjacent elements $\mathbf{E}_e$.

By the use of Lagrange's equation the equation of motion for an element is

$$\bar{\mathbf{M}}_e\ddot{\bar{\mathbf{U}}}_e + \bar{\mathbf{B}}_e\dot{\bar{\mathbf{U}}}_e + \bar{\mathbf{K}}_e\bar{\mathbf{U}}_e = \bar{\mathbf{P}}_e + \bar{\mathbf{g}}_e + \bar{\mathbf{E}}_e + \bar{\mathbf{F}}_e \tag{2.40}$$

All the above derivations have been carried out in a frame of reference local to the element. In order to apply this to a structure moving forward performing small oscillations about its mean position, we need to relate this to the frame that is fixed to the mean position of the hull. This can be done using the transformation matrix $\mathbf{L}$, which relates $\bar{\mathbf{U}}_e = \mathbf{L}\mathbf{U}_e$. $\mathbf{L}$ is a band matrix with submatrices $\mathbf{l}$ which, for small angles, can be approximated to

$$\mathbf{l} \approx \begin{bmatrix} 1 & \xi_6 & -\xi_5 \\ -\xi_6 & 1 & \xi_4 \\ \xi_5 & -\xi_4 & 1 \end{bmatrix} \tag{2.41}$$

where the rotation vector $\xi = (\xi_4, \xi_5, \xi_6)$ contains roll, pitch and yaw angles, respectively. The vector relation between the two frames is

$$\bar{\mathbf{u}} = \mathbf{l}\mathbf{u} \tag{2.42}$$

Recall that $\mathbf{l}$ and hence $\mathbf{L}$ are orthonormal matrices. Using this fact, we can write (2.40) in the equilibrium frame as

$$\mathbf{M}_e\ddot{\mathbf{U}}_e + \mathbf{B}_e\dot{\mathbf{U}}_e + \mathbf{K}_e\mathbf{U}_e = \mathbf{P}_e + \mathbf{g}_e + \mathbf{E}_e + \mathbf{F}_e \tag{2.43}$$

where $\mathbf{M}_e = \mathbf{L}^T\bar{\mathbf{M}}_e\mathbf{L}$ and $\mathbf{P}_e = \mathbf{L}^T\bar{\mathbf{P}}_e$. Since the gravity force is easy to express in this frame ($\mathbf{g} = -g\mathbf{k}$), it is now convenient to express the gravity component $\mathbf{g}_e$. The

virtual work is given by

$$\begin{aligned} \delta U_g = -\rho_b g \int_{\Omega_e} \delta \mathbf{u}^T \mathbf{k} d\Omega = -\rho_b g \int_{\Omega_e} \delta \bar{\mathbf{u}}_e^T \mathbf{l} \cdot \mathbf{k} d\Omega \\ = -\rho_b g \int_{\Omega_e} \delta \bar{\mathbf{U}}_e^T \mathbf{N}^T \mathbf{l} \cdot \mathbf{k} d\Omega = -\rho_b g \int_{\Omega_e} \delta \mathbf{U}_e^T \mathbf{L}^T \mathbf{N}^T \mathbf{l} \cdot \mathbf{k} d\Omega \end{aligned} \tag{2.44}$$

whence,

$$\mathbf{g_e} = -\rho_b g \int_{\Omega_e} \mathbf{L}^T \mathbf{N}^T \mathbf{l} \cdot \mathbf{k} d\Omega \tag{2.45}$$

Summing over all elements, we easily see

$$\sum_e E_e = 0 \tag{2.46}$$

at each node. The equation of motion (2.43) for the structure then takes the form

$$\mathbf{M}\ddot{\mathbf{U}} + \mathbf{B}\dot{\mathbf{U}} + \mathbf{K}\mathbf{U} = \mathbf{P} + \mathbf{g} + \mathbf{F} \tag{2.47}$$

$\mathbf{M}, \mathbf{B}, \mathbf{K}$ is structural mass, damping and stiffness, respectively. $\mathbf{P}$ is the pressure force, $\mathbf{g}$ is the gravity force and $\mathbf{F}$ represents point forces.

2.3.1 Natural frequencies and principal modes

If the are no damping or external forces acting, the equation of motion reduces to

$$\mathbf{M}\ddot{\mathbf{U}} + \mathbf{K}\mathbf{U} = \mathbf{0} \tag{2.48}$$

which has solutions of the form $\mathbf{U} = \mathbf{D}_r e^{i\omega_r t}$, where ω_r are the natural frequencies with eigenvectors $\mathbf{D}_r$. (Note that $D_r = [D_{r_1}, D_{r_2}, ..., D_{r_n}]$.) Each D_r represents a modeshape of the deflection. It is straightforward to show that $\mathbf{D_j}$ and $\mathbf{D_k}$ are orthogonal with respect to both $\mathbf{M}$ and $\mathbf{K}$ when $j \neq k$. If we let a submatrix $\mathbf{d_r}$ be formed for each element, then we can write

$$\mathbf{U}_{e_r} = \mathbf{d}_r e^{i\omega_r t} \tag{2.49}$$

and the modeshape at any point in the equilibrium frame is

$$\mathbf{u}_r(x,y,z) = \mathbf{l}^T\bar{\mathbf{u}}_{e_r} = \mathbf{l}^T\mathbf{N}\bar{\mathbf{U}}_{e_r} = \mathbf{l}^T\mathbf{N}\mathbf{L}\mathbf{d}_r e^{i\omega_r t} \tag{2.50}$$

Equation (2.50) gives the explicit transformation between the two frames of reference. If we let

$$\mathbf{U} = \mathbf{D}\mathbf{p} = \sum_{k=1}^{K} p_k(t)\mathbf{D}_k \tag{2.51}$$

and premultiply (2.47) by $\mathbf{D}^T$, then we can write the equation of motion as

$$\mathbf{m}\ddot{\mathbf{p}} + \mathbf{b}\dot{\mathbf{p}} + \mathbf{k}\mathbf{p} = \mathbf{Z} + \mathbf{G} + \mathbf{F}_p \tag{2.52}$$

where $\mathbf{m} = \mathbf{D^T M D}$, $\mathbf{Z} = \mathbf{D^T P}$ etc. At this stage, it is useful to investigate what $\mathbf{Z}$ actually is, since we have transformed and multiplied the pressure contribution several times. The rth component, corresponding to the principal coordinate p_r, is

$$\begin{aligned} Z_r = \mathbf{D}_r^T\mathbf{P} &= \textstyle\sum_e \mathbf{d}_r^T\mathbf{P}_e = \sum_e \mathbf{d}_r^T\mathbf{L}^T\bar{\mathbf{P}}_e = -\sum_e \mathbf{d}_r^T\mathbf{L}^T \int_{S_e} p\mathbf{N}^T\bar{\mathbf{n}}\, dS \\ &= -\textstyle\sum_e \mathbf{d}_r^T\mathbf{L}^T \int_{S_e} p\mathbf{N}^T\mathbf{l}\mathbf{n}\, dS = -\sum_e \int_{S_e} \mathbf{n}^T\mathbf{l}^T\mathbf{N}\mathbf{L}\mathbf{d}_r p\, dS \\ &= -\textstyle\sum_e \int_{S_e} \mathbf{n}^T\mathbf{l}^T\mathbf{N}\mathbf{L}\mathbf{U}_{e_r} p\, dS = -\int_S \mathbf{n}^T\mathbf{u}_r p\, dS \end{aligned} \tag{2.53}$$

which is exactly the expression for the generalized fluid force! This expression is exact, and needs to be linearized about the mean position of the body. A thorough linearization can be found in [20], [15]. The hydrodynamic part will be investigated further in Section 2.4.1, and the hydrostatic part will be linearized in Section 2.4.2.

The gravity influence will also have to be linearized. Consider the influence of gravity on mode r,

$$\mathbf{G}_r = -\sum_e \int \rho_b g w_r\, d\Omega = -\int_{\forall} \rho_b g w_r\, d\forall \tag{2.54}$$

where w_r is the w-component of the rth modeshape $\mathbf{u}_r = (u_r, v_r, w_r)$ and ρ_b is the density of the body. Write the difference between the exact position and the mean

position as

$$\int_{\forall} \rho_b g w_r d\forall - \int_{\forall_0} \rho_b g w_r \, d\forall \tag{2.55}$$

then the gravity influence in mode r due to a unit deformation in mode k is written

$$-G_{rk} = \int_{\Delta\forall_{0(k)}} \rho_b g w_r \, d\forall \tag{2.56}$$

when the density ρ_b is not dependent on spatial variables. $\Delta\forall_{0(k)}$ is the thin volume enclosed by the surfaces of the instantaneous body position and the mean body position. This volume can be approximated by the distance between the two surfaces S and $\bar{S}$, which is written $n_k = \mathbf{n} \cdot \mathbf{u}_k$.

$$-G_{rk} = \int_{\bar{S}} \rho_b g n_k w_r \, dS \tag{2.57}$$

and the total contribution is

$$G_r = -\int_{\forall_0} \rho_b g w_r \, d\forall - (\int_{\bar{S}} \rho_b g n_k w_r \, dS) \, p_k \tag{2.58}$$

In the special case were a rigid body mode is considered, this expression is identical to the form found in [20], [12].

2.3.2 Structural Dynamics - the Simple Way

In the previous sections of this chapter, a finite element approach was used to arrive at the coupled problem between fluid and structure. This approach is very mathematical and detailed, and some of the physical understanding is easily lost on the way. This section contains a straightforward derivation of the equation of motion, and serves both as a validation of the FEM method, and a more physical understanding of the problem. It will also prove useful for the examples presented later in this thesis. The basic assumption is that the structure can be modeled as a mass-spring-dashpot-system, which means that there are some stiffness (spring) and damping (dashpot) associated with the structure.

Consider a discretization of a body, partly or fully submerged. The equation of motion for the system can be described [8] by

$$\mathbf{M}\ddot{\mathbf{u}} + \mathbf{B}\dot{\mathbf{u}} + \mathbf{K}\mathbf{u} = \mathbf{f} \tag{2.59}$$

where $\mathbf{u} = \mathbf{u}(x, y, z, t)$ is the displacement vector described in the mean reference frame. **m,b,k** are the structural mass, damping and stiffness matrices, respectively. **f** is the external force acting on the body, including body forces, pressure forces and point forces, for instance.

Recall (2.51), and approximate the deformation of the body with K modeshapes $\mathbf{u}_k$, each with time-dependent amplitude $p_k(t)$,

$$\mathbf{u}(x, y, z, t) = \sum_{k=1}^{K} p_k \mathbf{u}_k(x, y, z) \tag{2.60}$$

Premultiply (2.59) with $\mathbf{u}_j^T$, and the following equations for the motions of the body are obtained:

$$\sum_{k=1}^{K} m_{jk}\ddot{p}_k + b_{jk}\dot{p}_k + k_{jk}p_k = F_j \qquad j = 1, ..., K \tag{2.61}$$

where $\mathbf{M}_{jk} = \mathbf{u}_j^T \mathbf{m}\mathbf{u}_k$ etc, and $F_j = \mathbf{u}_j^T \mathbf{f}$, hence the equation is equal to (2.52).

2.4 Force from the fluid

Still left is to evaluate the force on the body from the fluid, the component **Z** in (2.53). Before we can do this, the boundary-value problem outlined in Section 2.2 has to be solved. This will be solved by using a free-surface Green function and planar quadrilateral panels, where sources and dipoles are distributed over the body surface. This is a well known method, and is included in Appendix B for completeness.

All our equations are linearized and we assume that ship motions are time-invariant, then we can treat our system as a linear time invariant system, which simplifies the calculations tremendously. Using impulsive input signals, we compute canonical potentials ϕ_k for all modes. Convolution over time gives the response to an

arbitrary input signal. The radiation and the diffraction potentials take the form

$$\begin{aligned} \Phi_k &= \int_{-\infty}^{\infty} \varphi_k(t-\tau)\dot{p}_k(\tau)\, d\tau \\ \Phi_D &= \int_{-\infty}^{\infty} \varphi_D(t-\tau)\zeta(\tau)\, d\tau \end{aligned} \tag{2.62}$$

where ζ is the incoming wave amplitude. In (2.62) the canonical potentials are found from an impulsive velocity $\dot{p}_k = \delta(t)$. $\delta(t)$ is a delta function in time. Potentials can be calculated for any derivative of p, as shown by Bingham et al. [3].

2.4.1 Hydrodynamic force

The pressure force on the body in mode j due to an arbitrary forced motion in mode k is found from the linearized pressure integrated over the body. From the radiation potential we get

$$F_{jk} = -\rho \int_{\bar{S}} (\frac{\partial \Phi_k}{\partial t} - U\frac{\partial \Phi_k}{\partial x} + gz) n_j dS \tag{2.63}$$

The contribution due to the hydrostatic term $\rho g z$ will be evaluated in Section 2.4.2.

Consider first the pressure force due to the radiation potential Φ_k. A theorem attributed to Tuck [24] is in certain circumstances very useful,

$$\int_{\bar{S}} [m_j \Phi_k - n_j(\nabla\bar{\varphi} \cdot \nabla\Phi_k)] dS = -\int_{\bar{\Gamma}} n_j \Phi_k (\mathbf{l} \times \mathbf{n}) \cdot \nabla\bar{\varphi} \tag{2.64}$$

$\mathbf{l}$ is the unit vector tangent to the mean waterline. Calculation of the force using this theorem is done in Appendix C. Following Bingham et al. [3], each radiation potential can be decomposed

$$\varphi_k = \mathcal{N}_k(\mathbf{x})\dot{p}_k + \mathcal{M}_k(\mathbf{x})p_k + \psi_k(\mathbf{x}, t)h(t) \tag{2.65}$$

Note that summation does not apply. $h(t)$ is the Heaviside step function, and $\mathcal{N}_k$ and

$\mathcal{M}_k$ is found from the waveless problem

$$\begin{aligned} \nabla^2\mathcal{N}_k = 0 \qquad & \nabla^2\mathcal{M}_k = 0 \\ \mathcal{N}_k = 0 \qquad & \mathcal{M}_k = 0 \quad z = 0 \\ \mathbf{n}\cdot\nabla\mathcal{N}_k = n_k \quad & \mathbf{n}\cdot\nabla\mathcal{M}_k = m_k \quad \text{on } \bar{\mathrm{S}} \end{aligned} \tag{2.66}$$

Green's second identity gives the following integral equations for $\mathcal{N}_k$ and $\mathcal{M}_k$:

$$\begin{aligned} 2\pi\mathcal{N}_k + \int_{\bar{S}}(\mathcal{N}_k G_n^{(0)} - n_k G^{(0)})d\boldsymbol{\xi} = 0 \\ 2\pi\mathcal{M}_k + \int_{\bar{S}}(\mathcal{M}_k G_n^{(0)} - m_k G^{(0)})d\boldsymbol{\xi} = 0 \end{aligned} \tag{2.67}$$

When we calculate the radiation potential from impulsive velocity, the potential ψ_k satisfies

$$\begin{aligned} \nabla^2\psi_k = 0 & \\ \mathbf{n}\cdot\nabla\psi_k = 0 & \qquad \text{on } \bar{\mathrm{S}} \\ \mathcal{L}(\psi_k) = -g\tfrac{\partial\mathcal{M}_k}{\partial z} & \qquad z = 0 \\ \psi_k = 0 \qquad \tfrac{\partial\psi_k}{\partial t} = -g\tfrac{\partial\mathcal{N}_k}{\partial z} & \quad z = 0, t = 0 \end{aligned} \tag{2.68}$$

where $\mathcal{L}$ is the linearized free surface operator (2.14). For impulsive accelerations and displacements, the corresponding expression can be found in [2]. The general radiation potential Φ_k and its time derivative are

$$\begin{aligned} \Phi_k &= \mathcal{N}_k\dot{p}_k + \mathcal{M}_k p_k + \int_{-\infty}^{t}\psi_k(t-\tau)\dot{p}_k(\tau)\,d\tau \\ \tfrac{\partial\Phi_k}{\partial t} &= \mathcal{N}_k\ddot{p}_k + \mathcal{M}_k\dot{p}_k + \int_{-\infty}^{t}\tfrac{\partial\psi_k}{\partial t}(t-\tau)\dot{p}_k(\tau)\,d\tau \end{aligned} \tag{2.69}$$

Note again that summation does not apply. The force in the direction j due to a motion in the mode k due to the radiation pressure becomes

$$\begin{aligned} F_{jk} = -\rho\int_{\bar{S}}[(\mathcal{N}_k\ddot{p}_k + \mathcal{M}_k\dot{p}_k + \int_{-\infty}^{t}\tfrac{\partial\psi_k}{\partial t}(t-\tau)\dot{p}_k(\tau)\,d\tau)n_j \\ -U(\tfrac{\partial\mathcal{N}_k}{\partial x}\dot{p}_k + \tfrac{\partial\mathcal{M}_k}{\partial x}p_k + \int_{-\infty}^{t}\tfrac{\partial\psi_k}{\partial x}(t-\tau)\dot{p}_k(\tau)\,d\tau)n_j]\,dS \end{aligned} \tag{2.70}$$

Consider now the force due to diffraction. The canonical diffraction potential is

$\varphi_D = \varphi_I + \varphi_S$, and the potential's derivative can be expressed as

$$\frac{\partial \Phi_D}{\partial t} = \int_{-\infty}^{\infty} \frac{\partial \varphi_D}{\partial t}(t-\tau)\zeta(\tau)d\tau \tag{2.71}$$

and using (2.62) the force can be expressed as

$$\begin{gathered} F_{jD} = -\rho \int_{\bar{S}} (\tfrac{\partial \Phi_D}{\partial t} - U\tfrac{\partial \Phi_D}{\partial x}) n_j dS \\ = \int_{-\infty}^{\infty} [-\rho \int_{\bar{S}} (\tfrac{\partial \varphi_D}{\partial t}(t-\tau)n_j - U\tfrac{\partial \varphi_D}{\partial x}(t-\tau)n_j)\ dS]\zeta(\tau)\ d\tau \\ = \int_{-\infty}^{\infty} K_{jD}(t-\tau)\zeta(\tau)d\tau \end{gathered} \tag{2.72}$$

We will later use the notation

$$X_j(t) = \int_{-\infty}^{\infty} K_{jD}(t-\tau)\zeta(\tau)d\tau \tag{2.73}$$

At this stage, we have calculated the force due to the hydrodynamic pressure. Left is the task of evaluating the force due to buoyancy.

2.4.2 Hydrostatic force

In (2.63) the term $-\rho g z$ is the hydrostatic pressure. Calculations of the hydrostatic force due to this pressure for the rigid body are presented in [20], but for a general modeshape, a slightly different procedure is to be followed. We will not incorporate the contribution from body forces in the hydrostatic restoring matrix, since we will allow for random mass distribution in the analysis of generalized modes. The result of this procedure is different restoring coefficients in some modes, as an example in roll due to surge and sway. Usually these contributions are cancelled out by the gravity force. The restoring coefficient matrix will not be symmetric in general. The procedure is outlined in Newman [19].

$$F_i = -\rho \int_S g z n_i dS = -\rho \int_{\bar{S}} g z n_i dS - \rho \int_S g z n_i dS + \rho \int_{\bar{S}} g z n_i dS \tag{2.74}$$

We can express this in terms of a matrix C_{ij}, where $F_i = -\rho \int_{\bar{S}} dS\ gzn_i - C_{ij}p_j$, C_{ij} is the component of the force in the i direction due to a unit displacement of the body in the mode j, and we must sum over all modes j, $j = 1, ..., K$. We can define three surfaces of integration: the surface prior to the deformation is denoted $\bar{S}$, the deformed surface is $S_{\delta(j)}$ and η is the closed surface including the two former and the portion of the free surface $z = 0$ between the two, if they intersect the plane $z = 0$.

$$\begin{aligned} C_{ij} &= \rho g \int_{S_{\delta(j)}} zn_i dS - \rho g \int_{\bar{S}} zn_i dS = \rho g \int_{\eta} zn_i dS \\ &= \rho g \int_{\eta} z\mathbf{u}_i \cdot \mathbf{n} dS = \rho g \int_{\nu} \nabla \cdot z\mathbf{u}_i dV \end{aligned} \tag{2.75}$$

For small displacements the volume ν is thin, and can be approximated as the surface integral of the product of the integrand and the distance n_j between the two boundary surfaces.

$$C_{ij} \approx \rho g \int_{\bar{S}} n_j \nabla \cdot z\mathbf{u}_i dS = \rho g \int_{\bar{S}} n_j (w_i + zD_i) dS \tag{2.76}$$

where w_i is the w component of the modeshape vector $\mathbf{u}_i$ and $D_i = \nabla \cdot \mathbf{u}_i$ is the divergence of the same $\mathbf{u}_i$.

2.5 Equation of Motion

We are now able to write out all the components in (2.52). We assume that there are no point forces acting, $F_m = 0$. The equation of motion for $j = 1, ..., K$ can be written

$$\sum_{k=1}^{K} [(m_{jk} + A_{jk})\ddot{p}_k + (b_{jk} + B_{jk})\dot{p}_k + (k_{jk} + C_{jk} + c_{jk} + G_{jk})p_k] + \int_{-\infty}^{t} d\tau\ K_{jk}\dot{p}(\tau) = H_j + X_j \tag{2.77}$$

where the coefficients are

$$
\begin{aligned}
A_{jk} = &\quad \rho \int_{\bar{S}} dS\ \mathcal{N}_k n_j \\
B_{jk} = &\quad \rho \int_{\bar{S}} dS\ (\mathcal{M}_k - U\tfrac{\partial \mathcal{N}_k}{\partial x}) n_j \\
C_{jk} = &\quad \rho g \int_{\bar{S}} dS\ n_k (w_j + z D_j) \\
c_{jk} = &\quad -\rho \int_{\bar{S}} dS\ U \tfrac{\partial \mathcal{M}_k}{\partial x} n_j \\
G_{jk} = &\quad \rho g \int_{\bar{S}} dS\ n_k w_k \\
H_j = &\quad -\rho g \int_{\bar{S}} dS\ z n_j - \int_{\forall_0} \rho_b g w_j\ d\forall \\
X_j = &\quad \int d\tau\ K_{jD} \zeta(\tau) \\
K_{jD} = &\quad -\rho \int_{\bar{S}} dS\ (\tfrac{\partial}{\partial t}\Phi_D - U\tfrac{\partial}{\partial x}\Phi_D) n_j \\
K_{jk} = &\quad \rho \int_{\bar{S}} dS\ (\tfrac{\partial}{\partial t}\psi_k - U\tfrac{\partial}{\partial x}\psi_k) n_j
\end{aligned}
\tag{2.78}
$$

m, b, k are structural mass, damping and stiffness, respectively. Here n_j denotes the generalized normal vector $\mathbf{n} \cdot \mathbf{u}_j$. The term H_j includes contributions from 1st order hydrostatics and gravity. The coefficients calculated using Tuck's theorem can be found in Appendix C.

Chapter 3

Structural Deflection

3.1 Introduction

Consider a ship traveling in a seaway. Clearly, there must be moments and shear forces acting in the structure. These shear forces and moments result from deformation of the body, since the bending moment and the shear force scale like the second and third derivative of the deformation, as will be explained later. To see the deformation of a ship with the eye is usually hard, allthough in special cases it can be seen, for instance on Great Lake ships in rough seas. Measurements using strain gauges proves that some deformation takes place.

In order to study the deflection of a ship in waves, we will use the approach of generalized modes. We choose to use six rigid body modes to describe the motions (surge, sway, heave, roll, pitch, yaw) and some appropriate additional modes to describe the deformation. To illustrate the idea of generalized modes, we will study deformations and load distributions in the vertical plane only. Obviously, the best selection of modes to describe the deformation of a body is the eigenmodes of the structure, which can be obtained from (2.48). To find the eigenmodes for a general structure a finite element representation of the structure is required. Even then, we would only find the 'dry-modes'. The eigenmodes for the floating structure will be affected by the added mass, and would give the more physical 'wet-modes'. Fortunately, we do not have to restrict ourselves to any of these modes. Any set of modes

will do. The reason is that we are merely talking about a decomposition of a function, and that can always be done in a freely chosen basis. A set of pre-defined modes can therefore be used to describe the deformation of a given geometry, and we will demonstrate convergence for these modes.

A number of different types of modes can be used as input. A Fourier series is perhaps the simplest set of modes to use, and we can use Legendre polynomials, Chebyshev polynomials or free-free beam modes for instance. In general, convergence will be reached with fewer modes if the modes satisfy the boundary conditions of the equation of motion that describes the problem. It is also useful if they are orthogonal on some interval. An appropriate choice of interval will then cause off-diagonal terms to be zero in the linear system describing the motion, and reduce the computations needed to set up and solve the system. Convergence will also be reached faster if the modes chosen are 'close' to the physical modes. 'Close' means that the largest absolute error between the modeshape chosen and the natural mode is small. Another important criteria is that it will be useful if the analytical expression of the modes can be written down easily.

The free-free beam modes are given [7] as

$$u_{2j}(x) = \frac{1}{2}\left(\frac{\cos \kappa_{2j} x}{\cos \kappa_{2j}} + \frac{\cosh \kappa_{2j} x}{\cosh \kappa_{2j}}\right) \tag{3.1}$$

$$u_{2j+1}(x) = \frac{1}{2}\left(\frac{\sin \kappa_{2j+1} x}{\sin \kappa_{2j+1}} + \frac{\sinh \kappa_{2j+1} x}{\sinh \kappa_{2j+1}}\right) \tag{3.2}$$

in which x is a normalized coordinate, $x \in [-1, 1]$. The first two modes are $u_0 = 1$ and $u_1 = x$. The former is equal to heave, the latter is pitch-like. The factors κ_j are the real and positive roots of the equation

$$(-1)^j \tan \kappa_j + \tanh \kappa_j = 0 \tag{3.3}$$

The free-free beam modes are obtained as eigen solutions to a beam with no rigid support, when describing the deformation using Euler-Bernoulli theory. Hence, they satisfy the boundary conditions for a free beam (zero moment and shear force). The

free-free beam modes are orthogonal on $[-1,1]$. The modeshape vector as used in (2.24) is $\mathbf{u}_k = (0,0,u_k(x))$, and the boundary condition follows from (2.27). If we recall that the modeshape vector for pitch is $\mathbf{u}_5 = (z,0,-x)$ it is clear why the $u_1 = x$ is pitch-like. The distinction is, however, important in some applications, especially if the draft is comparable or larger than the length.

Another option is to use Legendre polynomials, given recursively [26] as

$$P_j(x) = \frac{(2j-1)xP_{j-1}(x) - (j-1)P_{j-2}(x)}{j} \tag{3.4}$$

where the two first modes are equal to the free-free beam modes, $P_0 = 1$ and $P_1 = x$. Legendre polynomials are also orthogonal on $[-1,1]$, but do not satisfy the boundary conditions for a free beam. The modeshape vector is now $\mathbf{u}_k = (0,0,P_k(x))$.

If forward speed of the body is considered, m-terms will be present and spatial derivatives of the modes will be required in (2.27). Derivatives of these two examples of modes are straightforward to obtain. Figures 3-1 to 3-4 present the modeshapes and their derivatives.

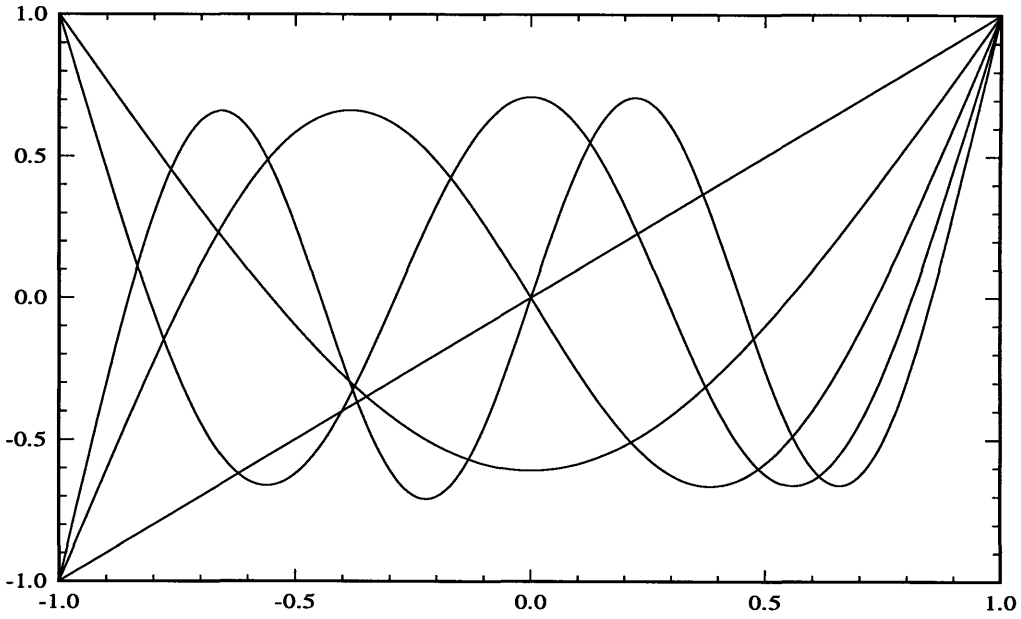

Figure 3-1: Free-free beam modes.

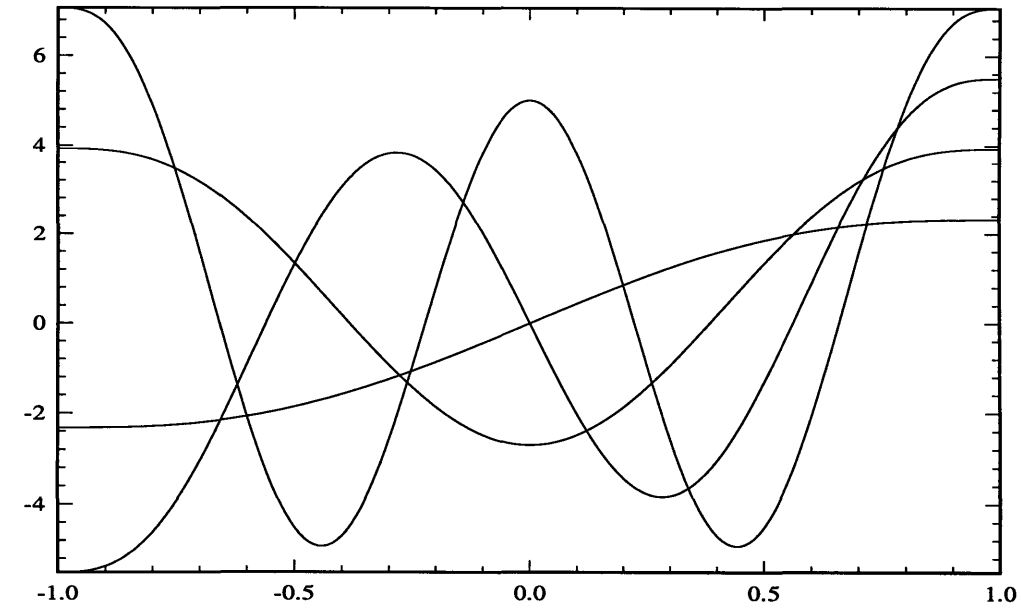

Figure 3-2: 1st derivative of the free-free beam modes to be used in the m-terms in the case of forward speed.

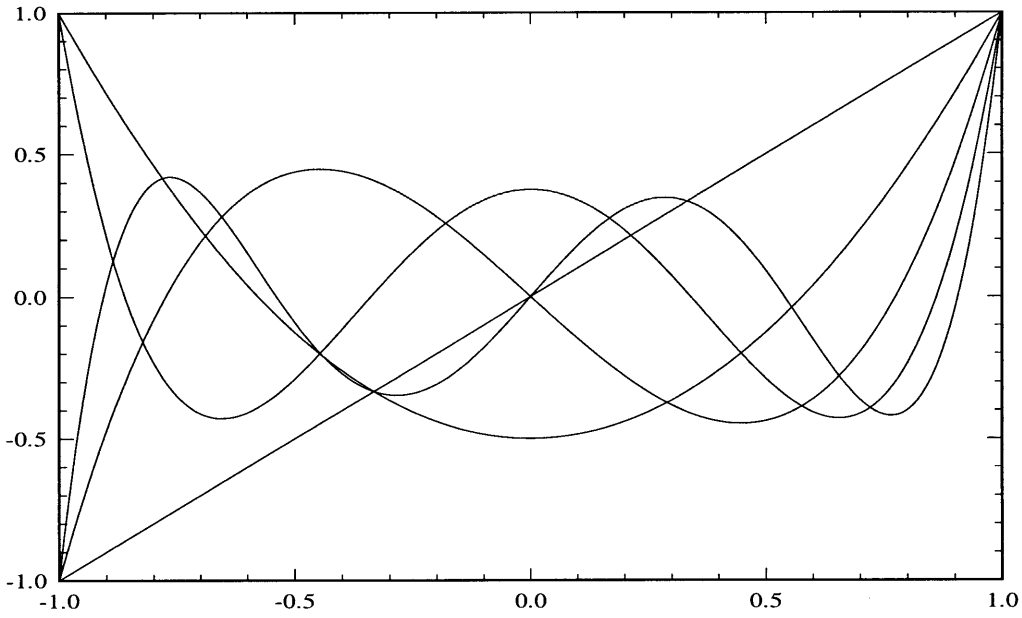

Figure 3-3: Legendre polynomials for use in structural deflection.

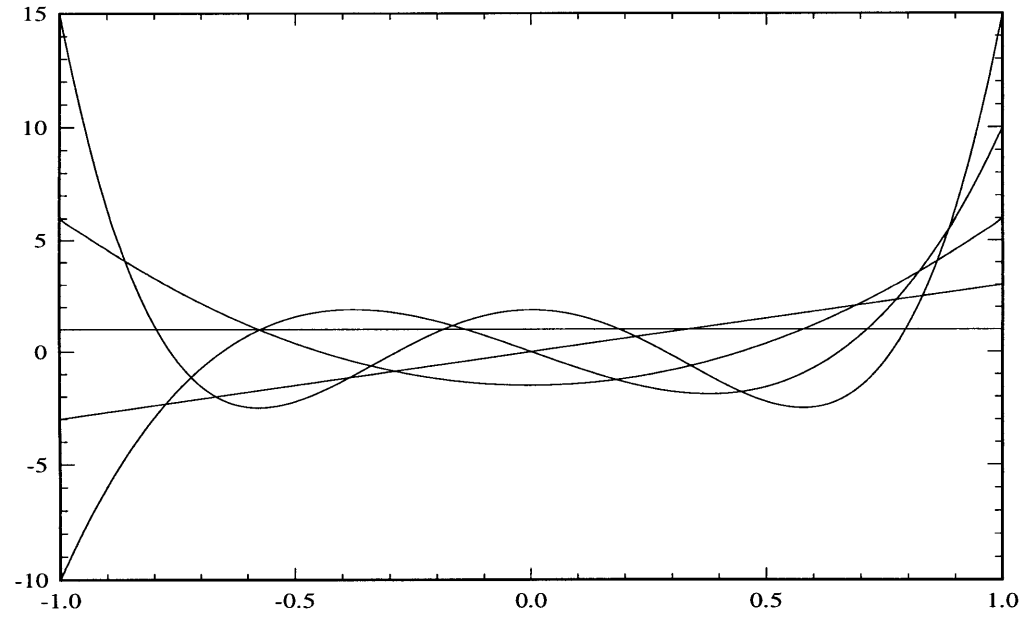

Figure 3-4: 1st derivative of the Legendre polynomials to be used in the m-terms.

3.2 Bending of a Slender Barge

The easiest way to represent the structural properties of a ship in a mathematical formulation is to consider it as a long slender, uniform beam. This approximation is, of course, very crude, but is still useful in illustrating how the idea of generalized modes can be used in the calculation of the structural deflections of the ship. Strip theory for the deformation of a long slender beam is well known from structural mechanics, here the Euler-Bernoulli theory will be used. A Timoshenko beam could also be used.

Consider a long slender beam of length L in a frame of reference fixed to the center of the undeflected beam. x is the longitudinal coordinate, the endpoints of the beam are at $x = \pm L/2$. z is the vertical coordinate, pointing upwards. Newton's second law in the vertical plane for a small piece of the beam takes the form

$$m\ddot{z} + \frac{d^2}{dx^2}(EI\frac{d^2z}{dx^2}) = F_z \tag{3.5}$$

where m is the mass of the section, E is Young's modulus and I the second moment of inertia. F_z is the external force in the z-direction, and d/dx is the derivative with respect to x. The boundary conditions describing no moment and shear force at the ends are

$$\frac{d^2z}{dx^2} = 0 \qquad \frac{d}{dx}(EI\frac{d^2z}{dx^2}) = 0 \qquad \text{at } x = \pm L/2 \tag{3.6}$$

Describing the deflection with a total of K modes, we write z as

$$z(x,t) = \sum_{j=1}^{K} p_j(t)w_j(x) \tag{3.7}$$

where w_j is the modeshape and p_j is the amplitude or the generalized coordinate. w is the z-component of the modeshape vector, $\mathbf{u}_j = (0, 0, w_j)$. Multiplying (3.5) by w_i gives

$$\sum_{j=1}^{K} w_i m w_j \ddot{p}_j + w_i \frac{d^2}{dx^2}(EI\frac{d^2w_j}{dx^2})p_j = w_i F_z \qquad i = 1, ..., K \tag{3.8}$$

and integrating over the length we get the equation of motion

$$m_{ij}\ddot{p}_j + k_{ij}p_j = Z_i \qquad i = 1, ..., K \tag{3.9}$$

where the mass matrix is defined by

$$m_{ij} = \int_{-L/2}^{L/2} w_i m w_j \mathrm{dx} \tag{3.10}$$

and the stiffness matrix by

$$k_{ij} = \int_{-L/2}^{L/2} w_i \frac{d^2}{dx^2}(EI\frac{d^2 w_j}{dx^2})\mathrm{dx} \tag{3.11}$$

The expression for the stiffness matrix element k_{ij} can be simplified by integrating by parts twice and invoking the boundary conditions (3.6). The expression is then

$$k_{ij} = \int_{-L/2}^{L/2} EI\frac{d^2 w_i}{dx^2}\frac{d^2 w_j}{dx^2}\mathrm{dx} \tag{3.12}$$

Both the mass matrix and the stiffness matrix are symmetric. If we consider a free vibration of the beam this can be simplified further, according to Bishop et al. [5]. If the beam is vibrating freely with a frequency γ_i corresponding to the i-th eigenmode, then

$$\frac{d^2}{dx^2}(EI\frac{d^2 w_i}{dx^2}) = m\gamma_i^2 w_i \tag{3.13}$$

Hence,

$$k_{ij} = \gamma_i^2 m_{ij}\delta_{ij} \tag{3.14}$$

Note that no summation is implied in (3.13) and (3.14). δ_{ij} is the Kronecker delta, $\delta = 1$ if $i = j$, $\delta = 0$ otherwise.

The forcing term Z_i in (3.9) is evaluated using the theory outlined in Chapter 2, and the final expression for the equation of motion is (2.77).

Newman showed in [19] that convergence was obtained for fewer modes when using the free-free beam modes than for Legendre polynomials or Chebyshev polynomials,

when performing calculations for a long, slender barge in the frequency-domain. Validation of the present, transient method can therefore be done by Fourier-transforming impulse response functions to get frequency-domain output. All calculations for the present method are done in an extension of the program TĪMIT [12], [4]. Frequency-domain quantities can also be obtained from the computer program WAMIT.WAMIT is a low order panel method program, which calculates the wave interactions with one or more bodies to regular waves, using a free-surface Green function formulation. The code has the capability to perform calculations for zero-speed problems in both finite and infinite depth. Further details can be found in [15], [13]. We will consider infinite depth only.

In the example we will use the free-free beam modes (3.1,3.2). The modes are, as aforementioned, orthogonal, and

$$\int_{-1}^{1} w_i(x)w_j(x)\mathrm{dx} = \frac{1}{2}\delta_{ij} \tag{3.15}$$

For a beam of length L with constant mass distribution m, the mass matrix takes the form

$$m_{ij} = m\int_{-L/2}^{L/2} w_i(2x/L)w_j(2x/L)\mathrm{dx} = \frac{1}{2}M\int_{-1}^{1} w_i(x)w_j(x)\mathrm{dx} = \frac{M}{4}\delta_{ij} \tag{3.16}$$

$M = mL$ is the total mass of the beam. The expression for the stiffness matrix is greatly simplified by the fact that the modes satisfy the differential equation

$$w_i^{(4)}(2x/L) - (\frac{2}{L}\kappa_i)^4 w_i(2x/L) = 0 \tag{3.17}$$

Assuming EI constant we now write k_{ij} as

$$k_{ij} = 4\frac{EI}{L^3}\kappa_i^4\delta_{ij} \tag{3.18}$$

and both the mass matrix and the stiffness matrix are diagonal. In the case of using other modeshapes that do not satisfy the boundary conditions, off diagonal entries

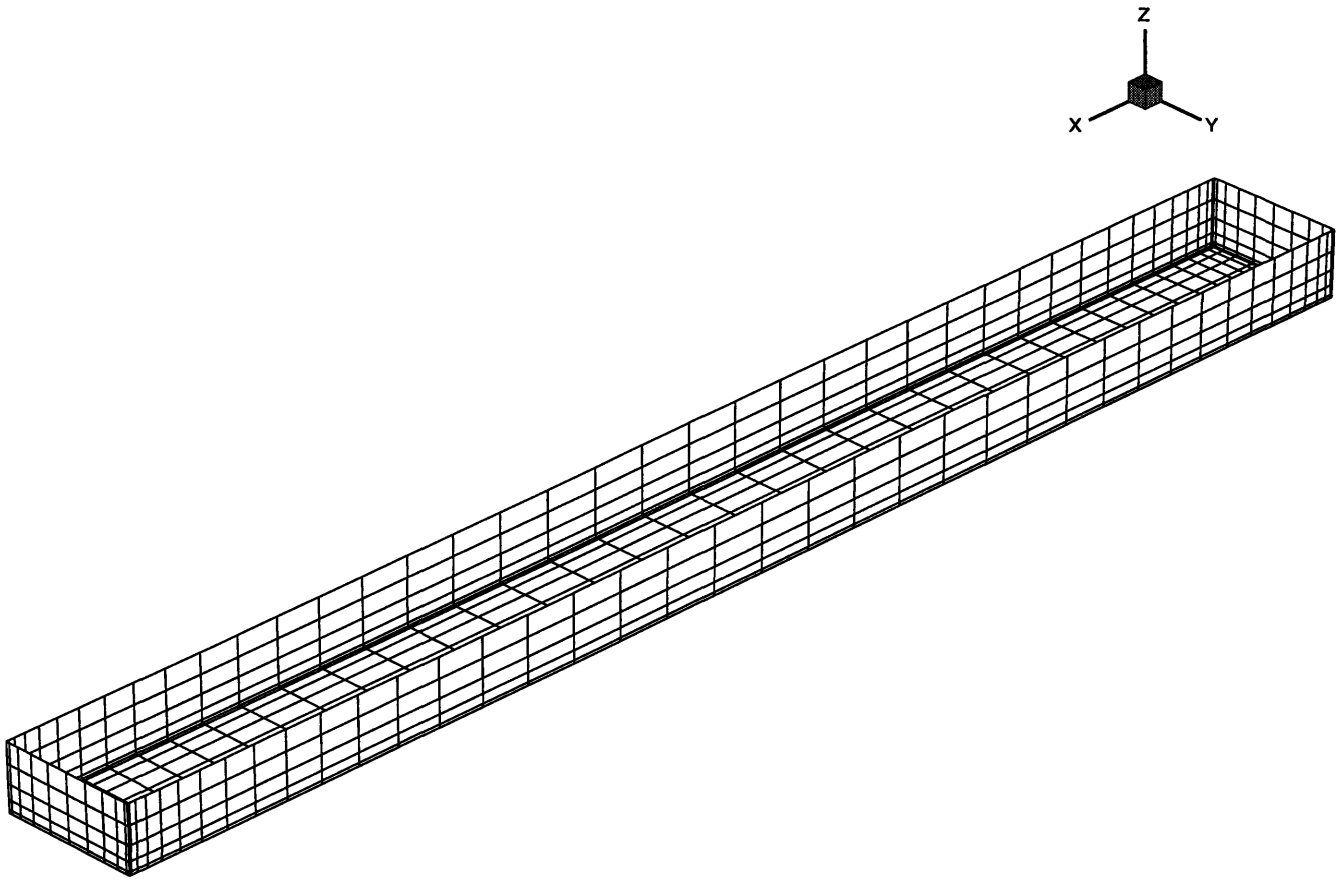

Figure 3-5: Discretization of the barge with 40 panels longitudinally, 5 vertically and 10 transversally. Total number of panels equals 900. Cosine spacing towards corners.

will occur in the stiffness matrix.

As an example, a calculation is done for a barge of length to beam ratio $L/B = 10$ and draft to beam ratio $T/B = 0.5$. The barge has zero speed. The total mass M equals the mass of the displaced volume, and the stiffness factor is $EI = 0.1ML^3/8s^2$. The barge is discretized with 900 panels, 40 longitudinally, 10 in the transverse direction and 5 in the vertical direction, and is presented in Figure 3-5. Cosine spacing is used towards the corners.

The figures 3-6 to 3-9 shows comparison between the present time domain calculations and frequency domain calculations for bending of the slender barge. The agreement between the two methods is excellent. This is however, no surprise. Korsmeyer et. al [13] showed in their paper that computations in the frequency domain

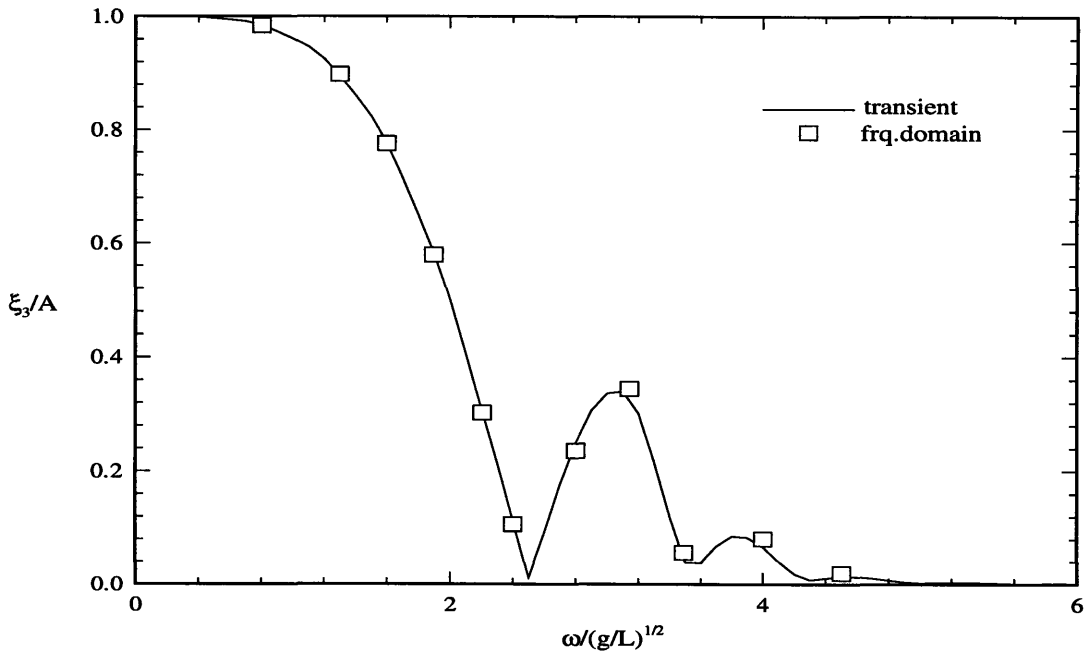

Figure 3-6: Heave RAO for a slender barge, calculated with 8 structural modes.

and in the time domain agreed within graphical precision. The two methods are based upon the same theory using a free-surface Green function, and this explains the excellent agreement. The response amplitude operator (RAO) is given as

$$\bar{\xi}_k = \frac{\xi_k}{A} \text{ k=1,2,3,7,8...} \qquad \bar{\xi}_k = \frac{\xi_k}{A/L} \text{ k=4,5,6} \tag{3.19}$$

where A is the amplitude of the forcing. k=1,2,3 are rigid-body translations and k=7,8,.. the deformation modes. The first deformable mode (k=7) corresponds to u_2 in (3.1). k=4,5,6 are the rigid-body rotations.

Table 3.2 contains the amplitude of each mode and the sum in each of eight bending modes for $\omega/(g/L)^{1/2} = 2.5$. This is the frequency of a wave with length approximately one ship length ($\omega = \sqrt{2\pi}$). The amplitude is calculated at the bow ($x = 1$). For this specific frequency, convergence to three decimals is achieved by using three modes.

Even if the two methods agree very well, there is a discrepancy that is notice-

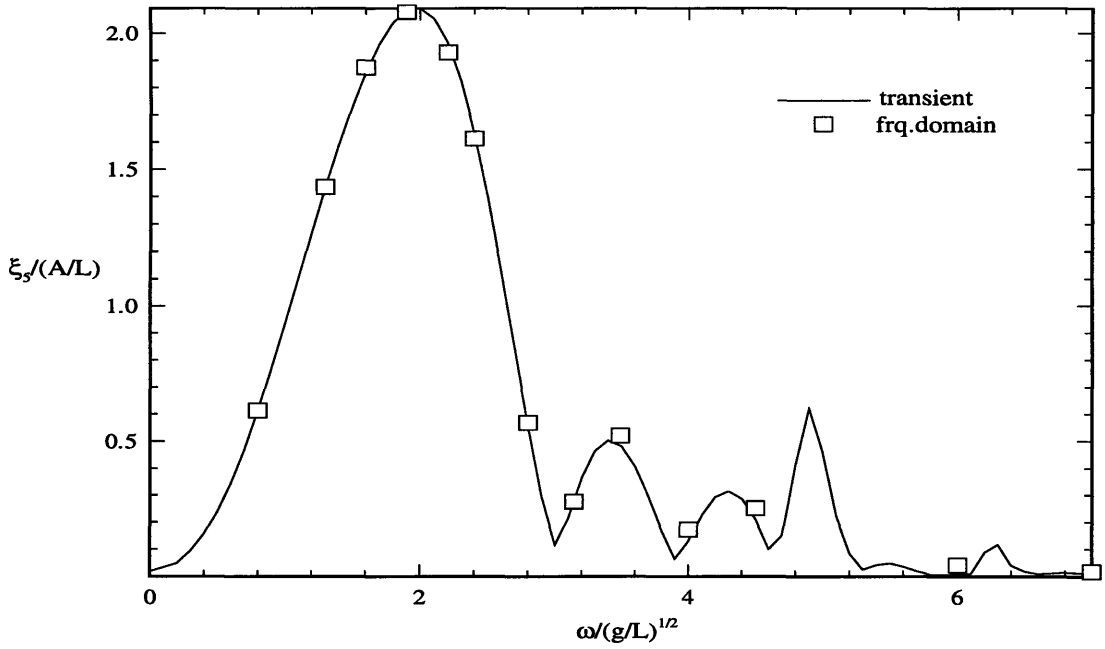

Figure 3-7: Pitch RAO for a slender barge, calculated with 8 structural modes.

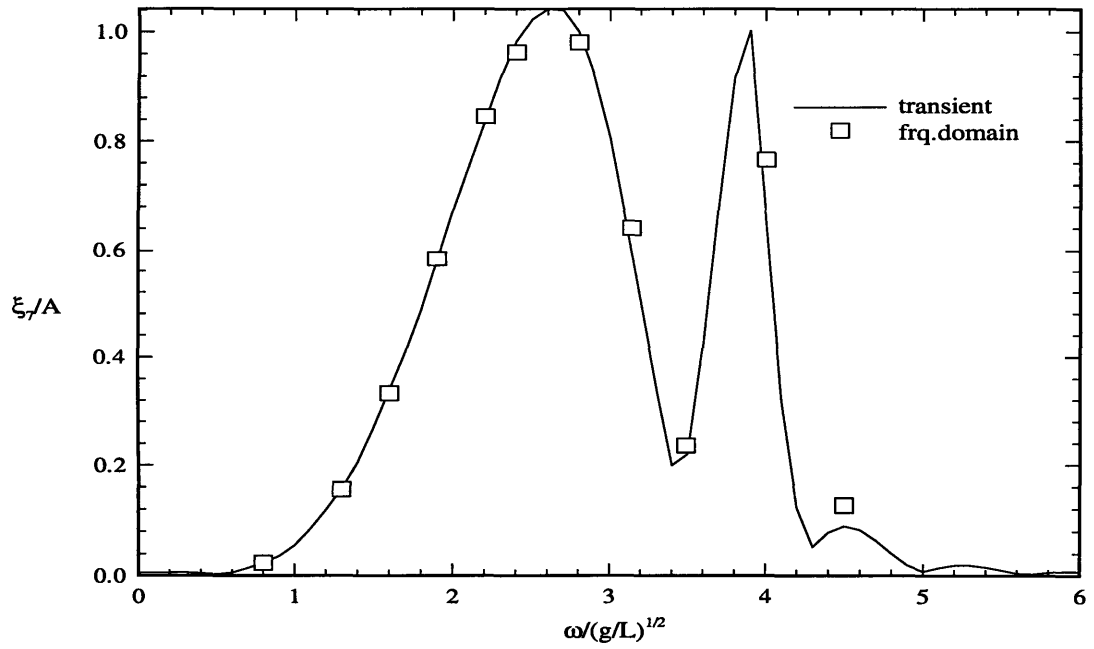

Figure 3-8: RAO for first structural mode, which represents hogging and sagging of the ship.

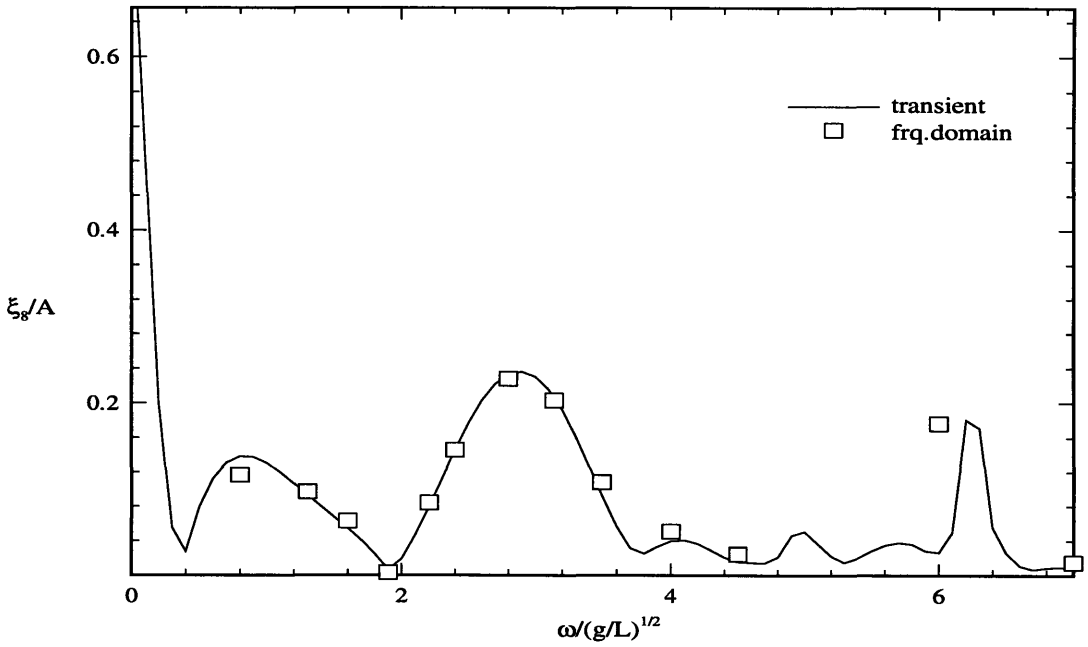

Figure 3-9: RAO for second structural mode.

	Beam modes		Legendre Polynomials	
Mode	$\lvert\xi_j\rvert$	Sum	$\lvert\xi_j\rvert$	Sum
7	1.022514	1.022514	1.137903	1.137903
8	0.1763145	1.039763	0.2288745	1.163583
9	1.3905380E-02	1.026030	0.1481183	1.018714
10	2.7216980E-03	1.026901	5.6185149E-02	1.007522
11	5.7292019E-04	1.026338	1.9562669E-02	1.026822
12	3.4398699E-04	1.026501	6.9660861E-03	1.027931
13	5.9705770E-05	1.026442	1.3769990E-03	1.026571
14	9.1134280E-05	1.026494	1.7360880E-04	1.026537

Table 3.1: Amplitude of each mode and sum (total deflection at the bow) for $\omega/(g/L)^{1/2} = 2.5$, using free-free beam modes and Legendre polynomials

able for the higher modes. The discrepancy in the low frequency limit for ξ_8 is most likely due to the asymptotic approximation of the large time behavior of the impulse response functions [4]. There is also a difference for both ξ_7 and ξ_8 for higher frequencies, as can be seen in Figures 3-8 and 3-9. The reason for this is not understood. Irregular frequencies are present in the this problem, but this is probably not the reason why the two results differ slightly. The common experience is that the two methods give the same results, even if they are incorrect due to inadequate spatial resolution of the high frequency content of the soultion.

Since the geometry in this example is simple, it is trivial to calculate the irregular frequencies for the problem. Following Newman et al. [22], the irregular frequencies occur when the potential ϕ inside the barge vanishes at the walls,

$$\phi = \left\{ \begin{array}{c} \cos \\ \sin \end{array} \right\} (k_x x) \cos(k_y y) \sinh(k(z+T)) \tag{3.20}$$

Here (k_x, k_y) are the components of the wavenumber with length k, the draft is T. The eigen solutions for the heave radiation problem are the symmetric parts of (3.20) and the anti-symmetric parts correspond to pitch. The irregular frequencies follow from

$$\frac{\omega^2}{g} = k \frac{\cosh(kT)}{\sinh(kT)} \tag{3.21}$$

and they occur for values of

$$k_y = \frac{2\pi}{B}(n + \frac{1}{2}) \qquad n = 0, 1, ... \qquad k_x = \frac{r\pi}{L} \qquad r = 1, 2, ... \tag{3.22}$$

Hence, there are infinetely many irregular frequencies, Table 3.2 lists the first. Most of these frequencies are outside the region of interest. Interpreting the results, it is important to keep in mind that irregular frequencies are present. However, it is not likely that the irregular frequencies are the reason for the discrepancy. This statement is based on the experience that the frequency-domain code and the time-domain code give the same results for the irregular frequencies when rigid-body modes

k_x	$k_y = \pi/B$	$k_y = 2\pi/B$	$k_y = 3\pi/B$
π/L	5.863301	9.711605	12.534397
$2\pi/L$	5.894928	9.719666	12.538154
$3\pi/L$	5.946786	9.733059	12.544408
$4\pi/L$	6.017673	9.751716	12.553148
$5\pi/L$	6.106033	9.775549	12.564360
$6\pi/L$	6.210068	9.804444	12.578021
$7\pi/L$	6.327850	9.838269	12.594109
$8\pi/L$	6.457415	9.876872	12.612597
$9\pi/L$	6.596851	9.920083	12.633451
$10\pi/L$	6.744361	9.967724	12.656637
$11\pi/L$	6.898302	10.019599	12.682117
$12\pi/L$	7.057207	10.075509	12.709847
$13\pi/L$	7.219800	10.135248	12.739785
$14\pi/L$	7.384985	10.198606	12.771884
$15\pi/L$	7.551840	10.265369	12.806091
$16\pi/L$	7.719601	10.335330	12.842358
$17\pi/L$	7.887640	10.408280	12.880630
$18\pi/L$	8.055452	10.484015	12.920852
$19\pi/L$	8.222636	10.562335	12.962967
$20\pi/L$	8.388876	10.643047	13.006920

Table 3.2: A number of irregular frequencies for a rectangular barge with L=1.0, B=0.1, T=0.05., obtained from the formula in (3.22).

are considered. Investigating Figure 3-8 we also find that the discrepancy occurs for a nondimensional frequency of 4.5, which is less than the lowest irregular frequency.

After obtaining the RAO's for all modes, we can write the deformation of the beam as a function $f(x)$

$$f(x) = \sum_{k=7}^{K} \xi_k w_k(x) \qquad x \in [\frac{-L}{2}, \frac{L}{2}] \tag{3.23}$$

The bending moment and shear force at any desired location is obtained by differentiation

$$M(x) = EI(x)\frac{d^2}{dx^2}f(x) \qquad V(x) = \frac{d}{dx}M(x) \tag{3.24}$$

Figure 3-10 presents the shear force at $x = -L/4$ and $x = L/4$ as a function of frequency. We note that for long waves the shear force at these two locations is

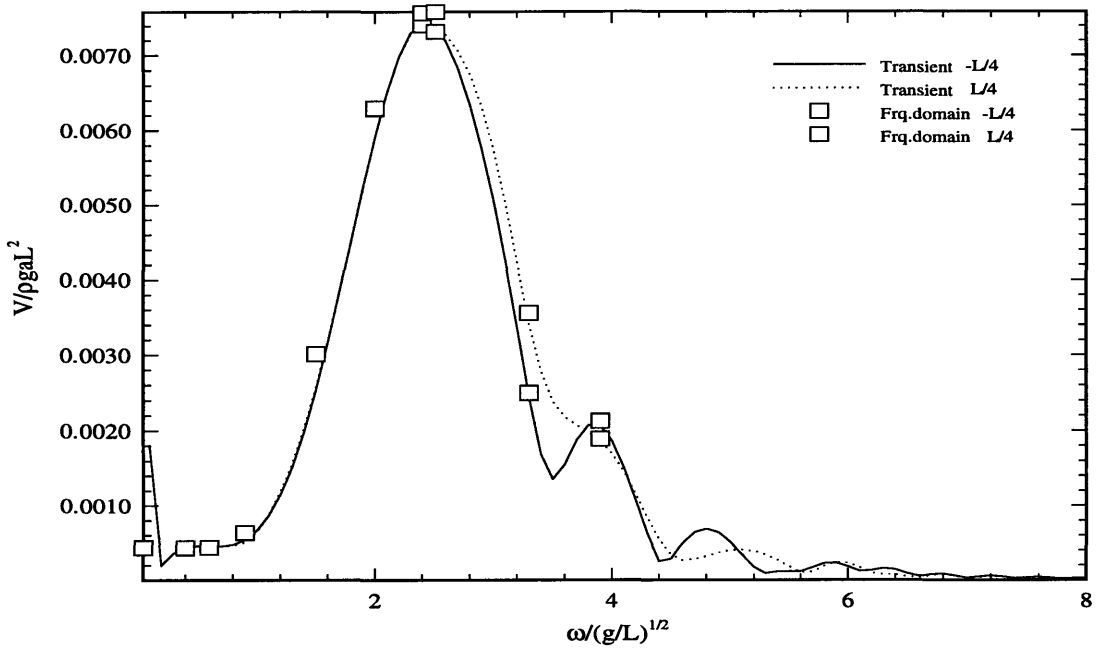

Figure 3-10: Shear force vs. frequency for the barge. -L/4 is aft of midships, L/4 is in front of midships.

symmetric, but for waves shorter than the length of the beam, the shear force is no longer symmetric. The explanation is that for long waves we will experience the Froude-Krylov part of the force only, and this is symmetric fore and aft. For shorter waves the flow pattern is no longer symmetric, since a sheltering effect is experienced.

The bending moment is presented in Figure 3-11. The maximum moment is for waves of about one ship length, which maximally excites the sag/hog condition.

Returning to the presented results for the shear force in Figure 3-10, we notice that in the low frequency limit, the shear force is not equal to zero, as one would expect. This can be traced back to the difficulties in calculating the low frequency response for the higher modes, as discussed previously in this chapter. For waves much longer than the structure itself, the shear force must be zero for floating bodies.

As mentioned earlier, frequency domain results from the transient calculations are obtained from a Fourier transform of the impulse-response function for each mode. The Fourier transform is performed using Filon integration as explained by Bingham

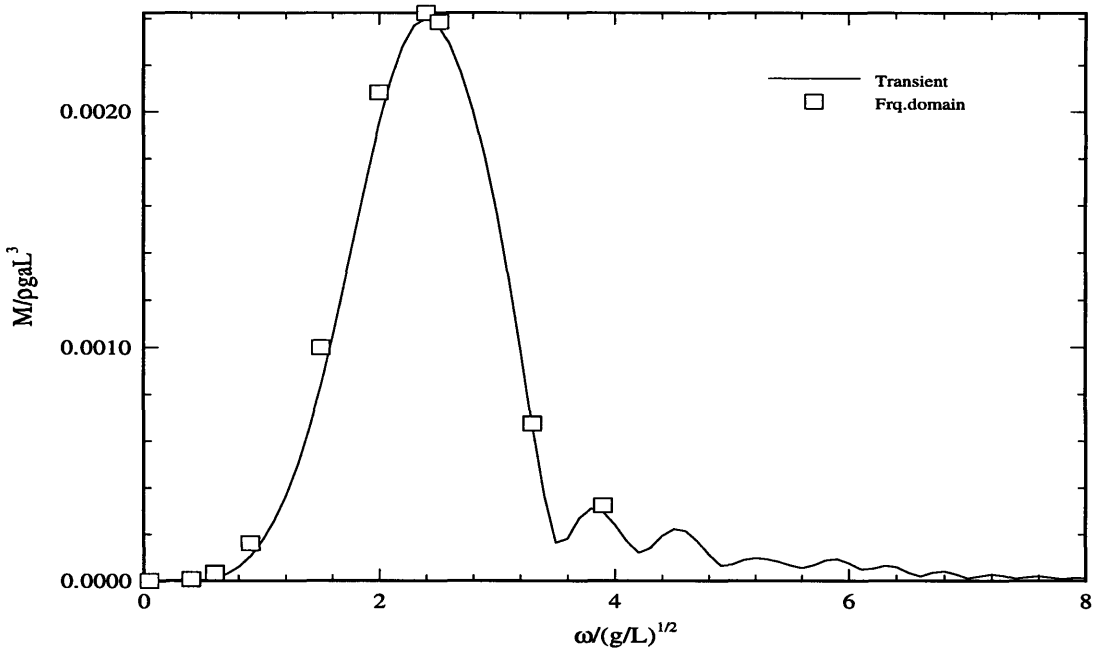

Figure 3-11: Bending moment at midships vs. frequency for the barge.

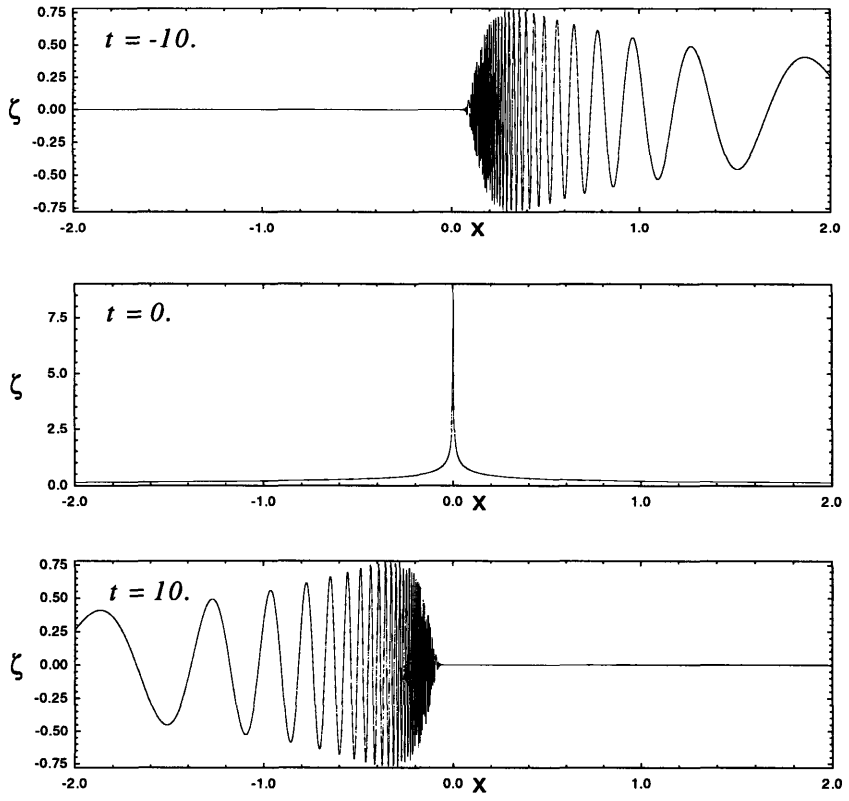

Figure 3-12: The impulsive incident wave elevation for zero speed.

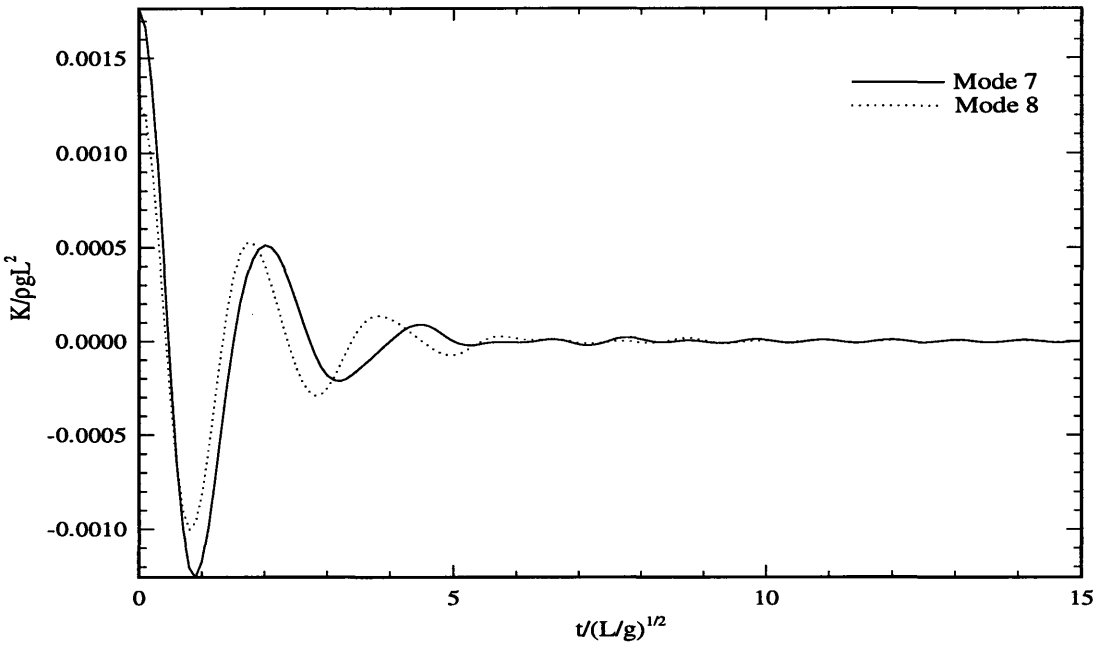

Figure 3-13: Radiation impulse-response function for first and second structural mode.

[4]. The diffraction impulse-response functions are calculated using an incident wave profile as seen in Figure 3-12. Radiation impulse-response are obtained by giving the body an impulsive velocity in the specified mode. Fourier transform of radiation impulse-response functions gives the added mass and damping, and Fourier transform of the diffraction impulse response gives the exciting force in the frequency-domain. Figure 3-13 shows the radiation impulse-response function for modes 7 and 8, corresponding to the first two deformable modes, Figure 3-14 shows the radiation impulse response function for the modes 9 and 10. We note that the area under each curve is decreasing with increasing mode-number. The area represents energy associated with the modeshape. As the energy decreases for higher modes, this must mean that the significance of the modes is decreasing.

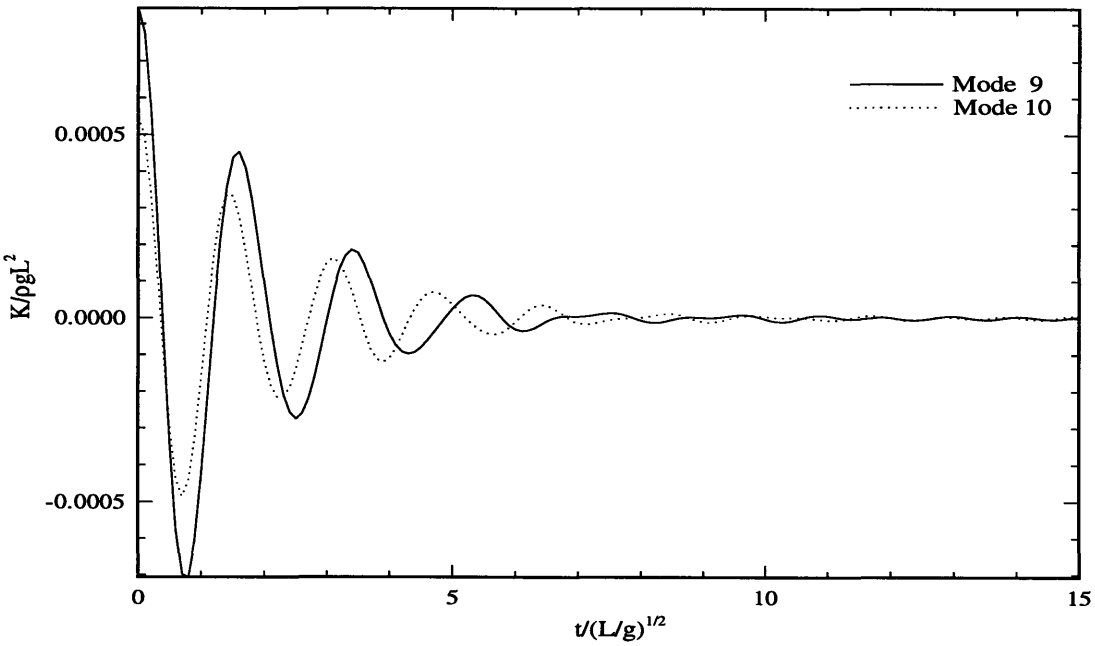

Figure 3-14: Radiation impulse-response function for third and fourth structural mode.

3.2.1 Modal Decomposition of the Load Distribution

So far we have investigated the hydroelastic deformation of a structure. Most structures and ships are stiff, however. "Stiff" means in this case that the ship does not deform very much compared to the rigid body motions. For instance, the amplitude of the heave motion is likely much larger than the deformation for a stiff ship. When this is true, we can neglect radiation due to deformation, and only consider the radiation from the rigid-body motions.

If we have a finite element model of the structure, the mass matrix and stiffness matrix are readily available, and we can easily perform hydroelastic analysis, and thereby obtain the loads we are interested in. However, if we put ourselves in the place of a designer, we need to know how strong the structure has to be before we design the structure. In this situation is it useful to perform computations based on the hydrodynamic loads on the undeformed ship. The common practice in naval architecture is to calculate bending moments and shear stresses based on certain

static criteria, where the form of the hull and various wave lengths are not taken into account [25]. The method presented in this section takes into account the diffraction and radiation when calculating the moments and shear stresses.

Consider some continuously diffrentiable function $f(x)$ $x \in [-1, 1]$. Any such function can be decomposed using a set of orthogonal basis-functions. Then we can write

$$f(x) = \sum_{i=0}^{\infty} C_i P_i(x) \tag{3.25}$$

The basis functions $P_i(x)$ are known, the unknowns are the coefficients C_i. With some manipulation we find that

$$\int_{-1}^{1} f(x)P_j(x)\mathrm{dx} = \int_{-1}^{1} \sum_{k=0}^{\infty} C_i P_i(x)P_j(x)\mathrm{dx} = C_j \int_{-1}^{1} P_j^2(x)\mathrm{dx} \tag{3.26}$$

since the basis functions are orthogonal. If the basis functions are orthonormal, then the latter integral is equal to unity.

If we return to (3.5) and write Newton's second law for a small strip of the structure, but now in a slightly different way,

$$m\ddot{z} + \frac{dV}{dx} = F_z \tag{3.27}$$

where m is the sectional mass, V the shear force, and F the external forcing, we immediately notice that if we can find $\frac{dV}{dx}$, the shear forces and bending moments can be found from integration.

Let $l(x) = \frac{dV}{dx}$, and write $l(x)$ as

$$l(x) = \sum_{i=0}^{\infty} D_i P_i(x) \tag{3.28}$$

Since $l(x)$ must satisfy the equilibrium conditions

$$\int_{-1}^{1} l(x)\mathrm{dx} = 0 \qquad \int_{-1}^{1} xl(x)\mathrm{dx} = 0 \tag{3.29}$$

it follows that D_0 and D_1 must be zero. We now re-write (3.27) as

$$l(x) = F_z(x) - m\ddot{z} \tag{3.30}$$

Premultiplying by P_j and integrating over the length of the structure, we find

$$D_j \int_{-1}^{1} P_j^2(x)\mathrm{dx} = k_{jk}p_k = X_j - (-\omega^2(A_{jk} + m_{jk}) + i\omega B_{jk} + C_{jk})p_k \tag{3.31}$$

where k_{jk} is the stiffness matrix, ω is the absolute wave frequency, A_{jk} is the added mass, m_{jk} is the mass matrix, i is the imaginary unit , B_{jk} is the damping, C_{jk} is the hydrostatic restoring and X_j the exciting force coefficient. This means that if we have the stiffness and the RAOs for all modes, we can easily find the coefficients D_j.

However, as the stiffness is becoming large and the deflections small, the product $k_{jk}p_k$ will become difficult to evaluate. The right-hand side of (3.31) can be approximated by summing over $k = 1, .., 6$, since $p_k, k \geq 7$ is assumed small compared to the rigid-body motion. To get a reasonable approximation, all we need to know is the rigid-body motion of the structure and the coupling terms between rigid-body motion and deflections for added-mass, damping and hydrostatic restoring. We need to know the terms which contain information about added-mass and damping in deformable modes due to rigid-body motion only, but not the other way.

Using this approach, we can investigate the global loads in a long, slender, stiff beam. We are using the same discretization as shown in Figure 3-5. We do not need to perform new hydrodynamic calculations, we are merely interested in post processing these quantities to obtain the load distribution. We still use a constant stiffness, but we use a much larger value for the stiffness $EI = 400 * ML^3/8s^2$. Figure 3-15 clearly demonstrates that this method works. In this figure, one of the load distributions is calculated using the hydroelastic method, whereas the other distribution is calculated using the "stiff" approach. Figure 3-16 shows the corresponding real and imaginary parts. Eight free-free beam modes were used in this example, in general convergence has been found for less than 10 modes.

The graphical difference between the two methods is clear, but it is small. And

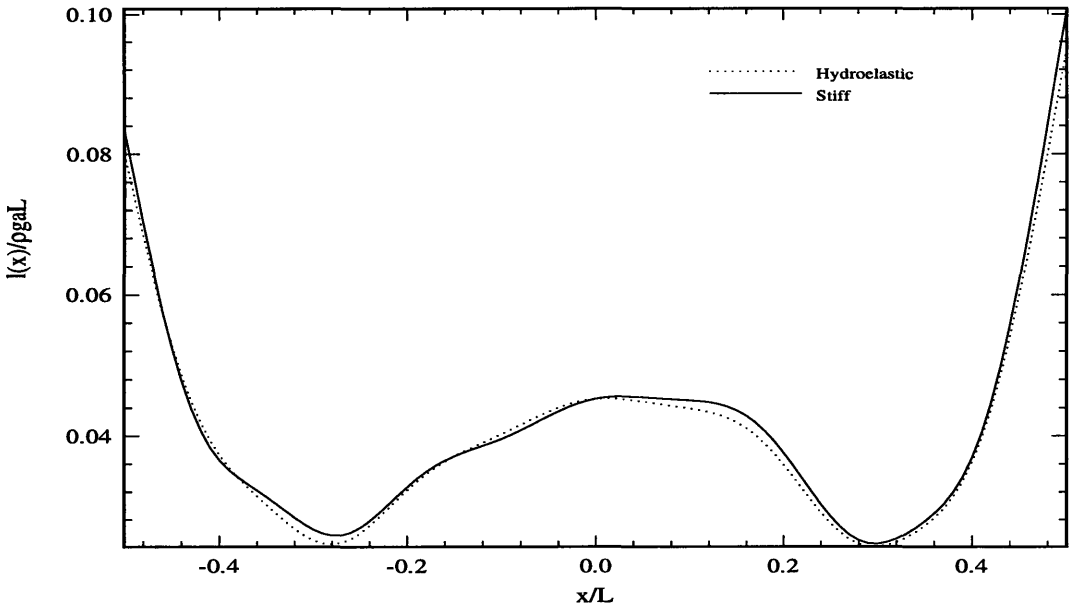

Figure 3-15: Load distribution for the slender barge for $\omega = 2.5$, head seas. Solid line is distribution calculated using the "stiff" approach, dotted line is hydroelastic calculation.

the stiffness factor EI used for this calculation is probably in some mid-range when considering stiffness of real structures. As the stiffness increases, we expect to find that the two results converge.

3.3 Bending of a Wigley Hull

3.3.1 Zero Speed

Based on the analysis and validation of the method described in the previous section, we can proceed to a more realistic hull shape, and also include forward-speed effects. Throughout this section we will study the global loads on a Wigley Hull. Figure 3-17 presents the hull form with a total of 1600 panels. The characteristics are L/B=10, and L/T=20, where L is the length, B the beam and T is the draft.

The form of the hull is more complex than the barge, and obtaining an expression for the stiffness element k_{jk} is not straightforward. If we had a finite element

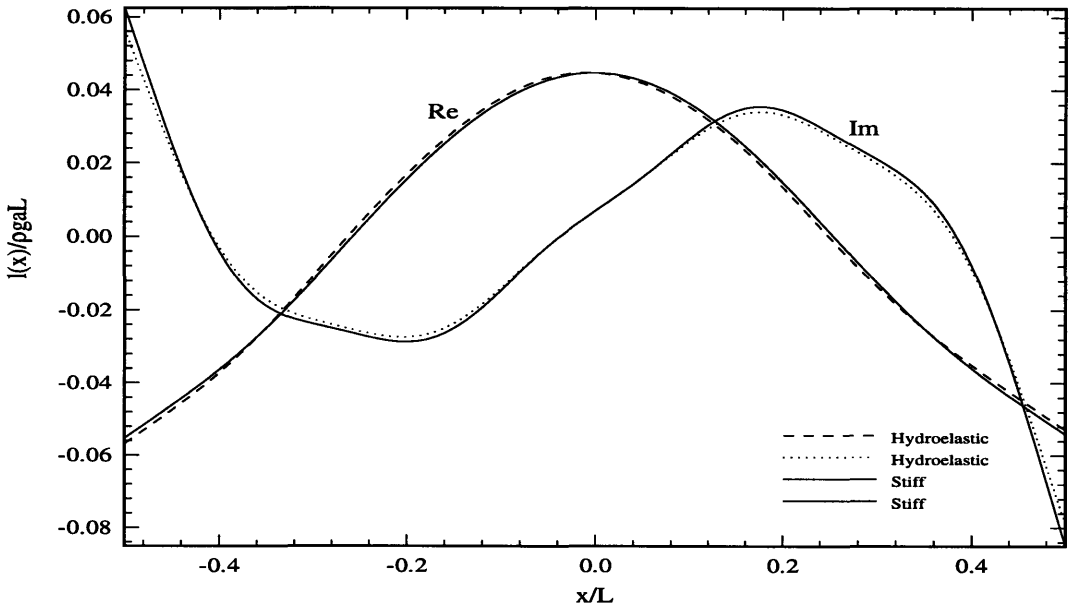

Figure 3-16: Load distribution for the slender barge for $\omega = 2.5$, head seas. Solid line is distribution calculated using the "stiff" approach, dotted line is hydroelastic calculation. The figure presents the real and imaginary parts.

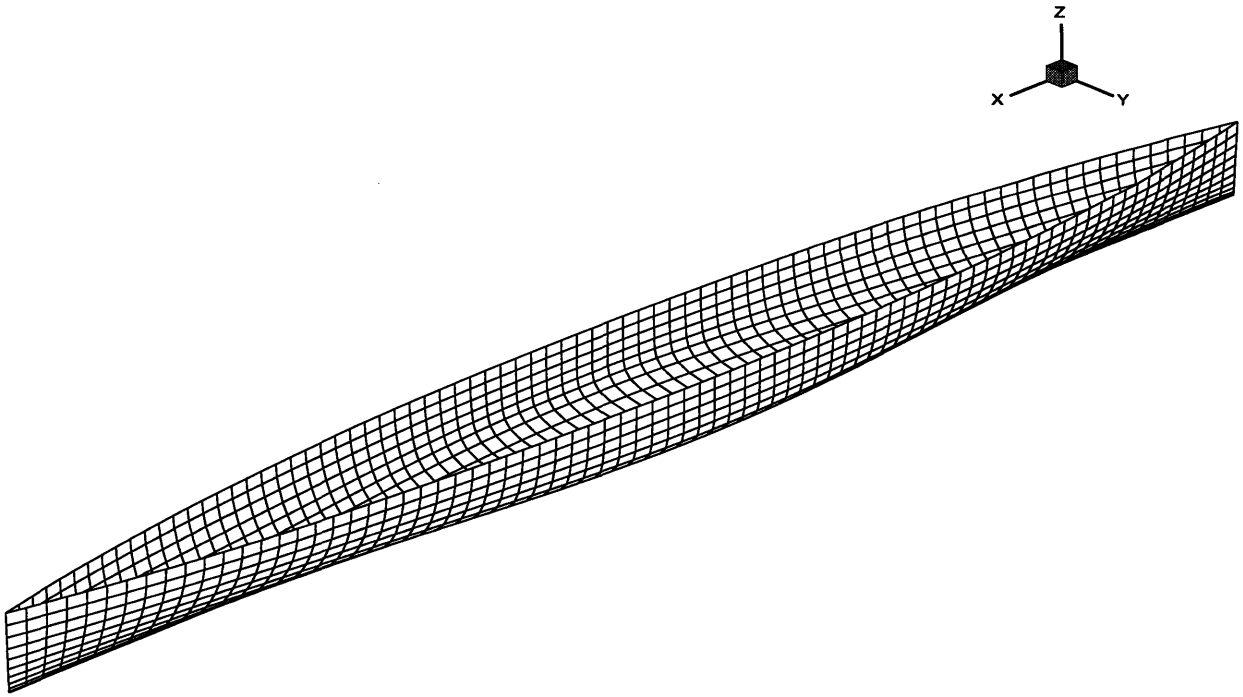

Figure 3-17: Wigley hull with 1600 panels overall. There are 80 panels longitudinally and 20 along the girth.

model of the structure, this could have been used to calculate the stiffness. We could then perform a hydroelastic analysis. Since the stiffness matrix is not available, an analysis under the assumption that the ship is stiff is appropriate. Performing the hydrodynamic analysis and utilizing the flexibility in the generalized modes theory, we can find the quantities necessary to calculate the coefficients in (3.31). If we consider forward-speed, an additional term of hydrodynamic restoring will enter in the equation(3.31) , as it does in the equation of motion (2.77).

To perform calculations of the global loads, we need the mass distribution of the ship. In the example to follow, the mass is assumed distributed as the local beam, scaled so that the weight of the total mass equals the mass of the displaced fluid. In Figure 3-18 and Figure 3-19 the global loads are presented for zero speed in head seas. We again notice that there is a difference in the shear force at $x = -L/4$ and $x = L/4$ as we experienced with the barge. The sheltering effect is stronger for the Wigley hull, due to its geometry. The bending moment behaves in the same way as we found with the beam, with two differences that are important to note: the magnitude is about half for the Wigley hull compared to the beam, and the maximum bending occurs for waves that are slightly shorter than the length between the perpendiculars. The maximum value is found for a non-dimensional frequency ω of about 2.8, which corresponds to a wavelength of $0.8L$. This could be anticipated from the geometry of the Wigley hull, since it has zero beam at the ends, maximum hog and sag are experienced for waves which are shorter than the ship length. This trend applies for the wavelength of the maximum shear force as well.

3.3.2 Forward Speed

In this section results for a Wigley Hull traveling in head seas with $Fn = 0.3$ are presented. In general there will be a difference between the absolute frequency of the wave and the encounter frequency experienced by the ship when forward speed is considered. The relation between the encounter frequency ω_e and the absolute wave

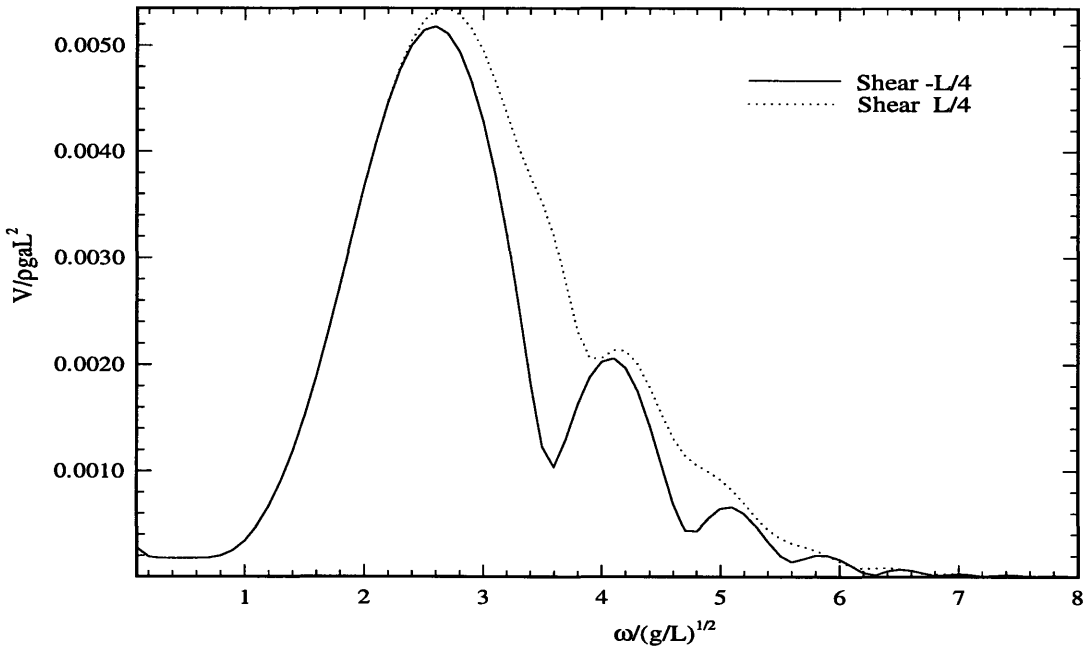

Figure 3-18: Shear force at x=-L/4 and x=L/4 for a Wigley Hull in head seas, Fn=0.0.

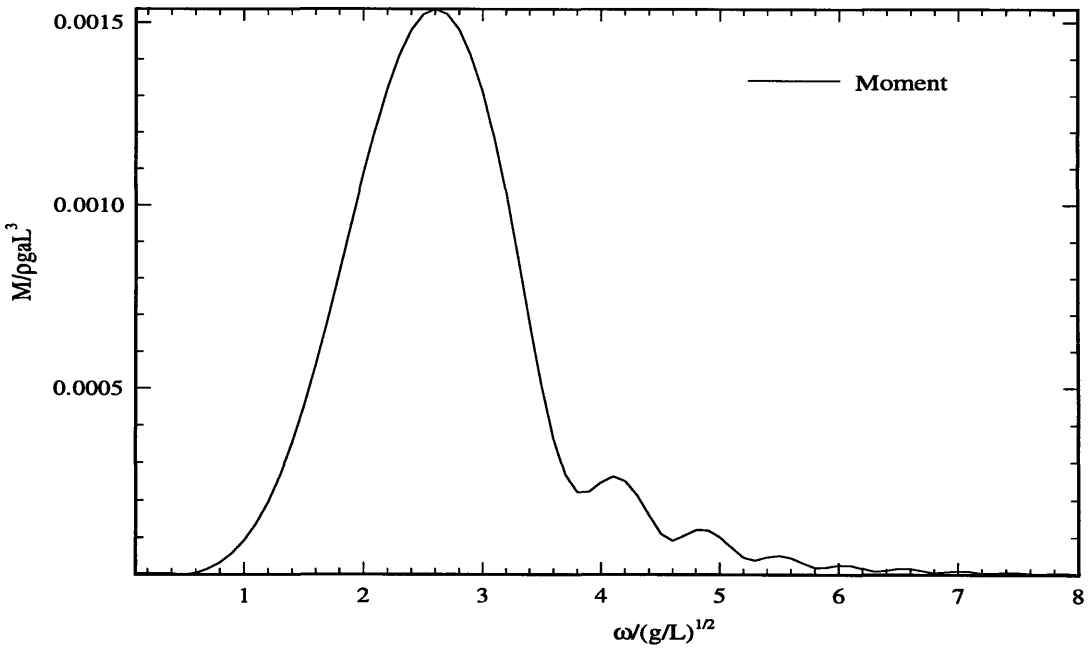

Figure 3-19: Bending moment at midship for a Wigley Hull in head seas, Fn=0.0.

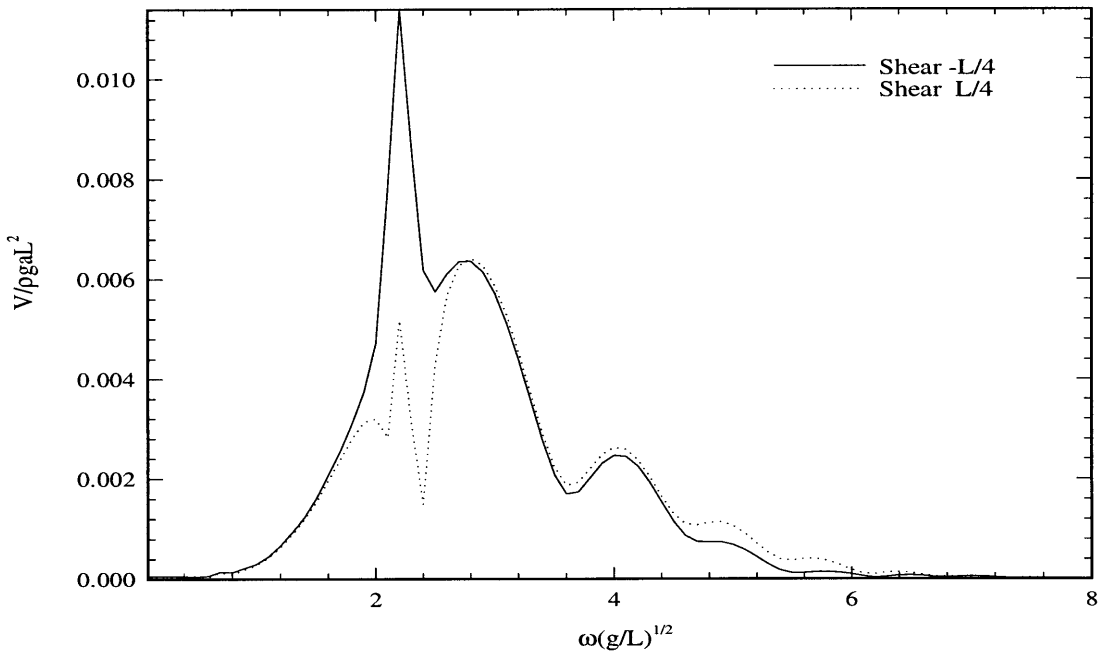

Figure 3-20: Shear force at x=-L/4 and x=L/4 for a Wigley Hull in head seas, Fn=0.3, as a function of absolute frequency.

frequency ω_0 is

$$\omega_e = \omega_0 - \omega_0^2 \frac{U \cos\beta}{g} \tag{3.32}$$

where β is the angle between the incoming wave and the ship, 180^o is head seas, U is the ship speed and g gravity.

In Figure 3-21 the bending moment at midship is presented and in Figure 3-20 the shear force at $x = -L/4$ and $x = L/4$.

The effect of the forward speed is quite large. The peak magnitudes of both the bending moments and the shear forces are approximately twice the value for zero speed. The distribution is also different. We find that the peak values are shifted towards longer waves, this is related to the fact that the frequencies for the peak values are closely related with the corresponding frequencies for heave and pitch. When considering head waves and forward speed, the frequency of encounter is higher than the absolute frequency of the waves, hence the wave-frequencies for maximum amplitude of the motions and loads are shifted towards longer waves.

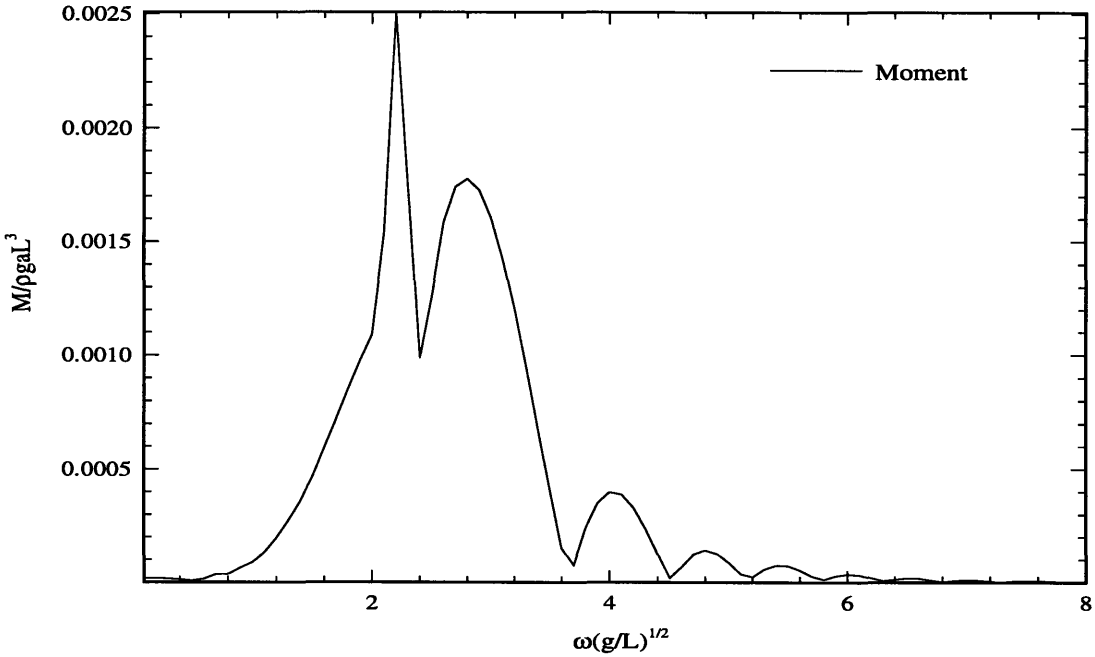

Figure 3-21: Bending moment at midship for a Wigley Hull in head seas, Fn=0.3, as a function of absolute frequency.

The shape of the distribution has also changed significantly from the zero-speed case. A shape of the transfer function with two maxima is experienced for both bending and shear forces. The peak value which corresponds to the lowest frequency is associated with inertia effects, the peak for higher frequencies is dominated by hydrodynamic effects.

Figures 3-22 and 3-23 presents the same values for the shear force and bending moment, but now as a function of the encounter frequency. The transformation between absolute frequency and encounter frequency is non-linear, here this means a non-linear stretching of the coordinate. Studying these results, we find that the bandwidth where most of the energy is contained, is larger for the encounter frequency at forward speed than for zero speed. At zero speed this interval is from a non-dimensional frequency of about 1 to 4 with a bandwidth of 3, where as the corresponding bandwidth for forward speed is about 6.5, and the energy is contained within the interval from 1 to 7.5. No firm conclusion can be drawn based on these

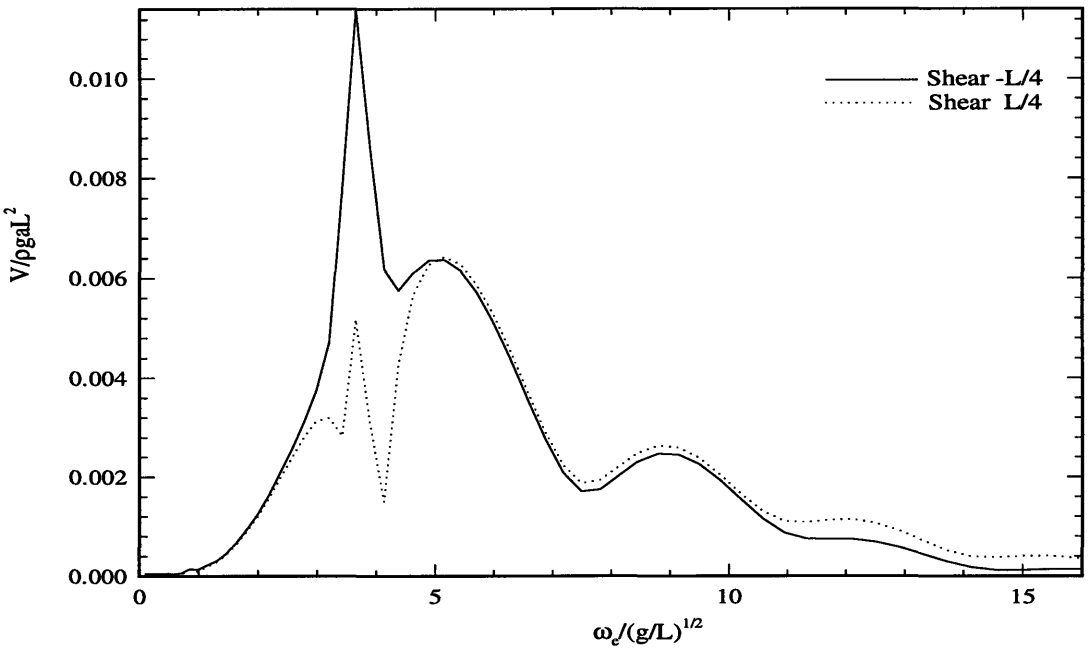

Figure 3-22: Shear force at x=-L/4 and x=L/4 for a Wigley Hull in head seas, Fn=0.3, as a function of encounter frequency.

results, but it is clear that both the absolute frequency of the wave ω_0 and the encounter frequency ω_e is important. This statement is also supported by the fact that the exciting force coefficient (2.73) is a function of the encounter frequency, but that the radiation potential is a function of ω_0 only.

3.4 Comparison with Experiments

For validation of the method to calculate the bending moments and shear stresses, comparison has been done with experiments carried out by Adegeest [1]. In the experiments two different hulls were tested to investigate the effect of bow flare on the motions and the loads. Both hulls had the same underwater hull, identically to the Wigley hull. One had bow flare, the other had not. In the present, transient, linear method, there is of course no way to capture the effect of the bow flare above the waterline, so we can only compare the results for the original Wigley hull. Comparison has been done for the bending moment at midships.

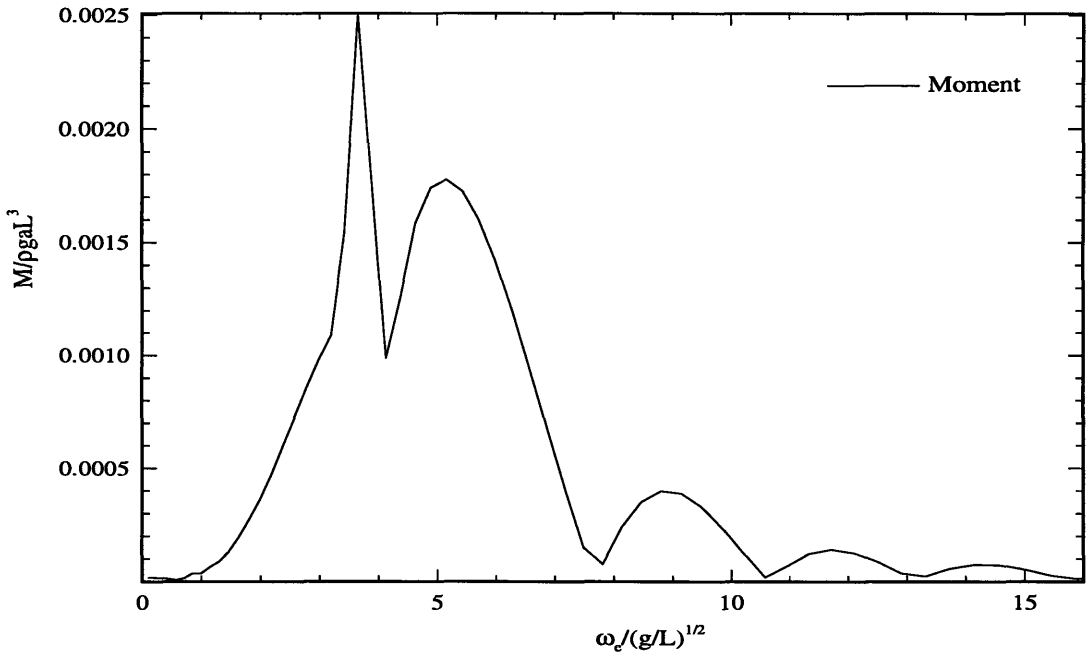

Figure 3-23: Bending moment at midship for a Wigley Hull in head seas, Fn=0.3, as a function of encounter frequency.

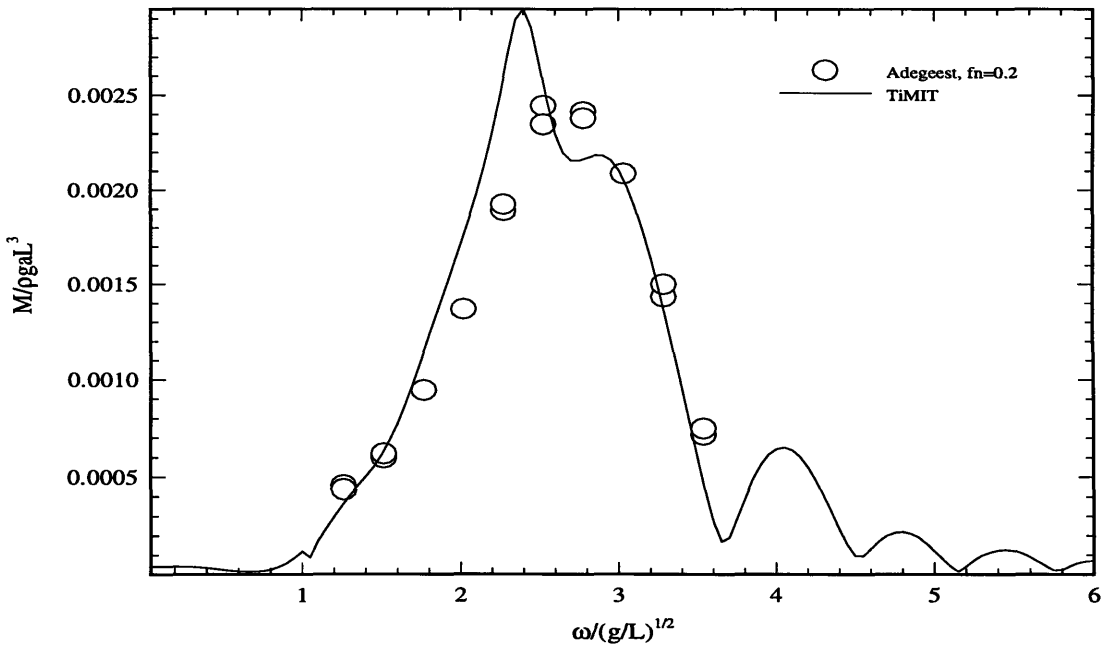

Figure 3-24: Comparison of the bending moment at midships for the Wigley hull used by Adegeest in head seas, Fn=0.2.

Adegeest used L/B=7 an L/T=18. L is the length, B the beam and T the draft, and the actual ship-length was 2.5 m. The wave amplitude was in the range 2-3 cm for waves of frequency up to 7Hz. The mass-distribution used in the comparison satisfies the distribution specified from the experiments, the center of gravity and the radii of gyration for each of the three sections the hull were made up of. The calculation was then done using 8 free-free beam modes, and calculating the load-distribution over the hull using (3.31).

As is shown in Figure 3-24, the comparison between the two methods is quite good. Error is only found for the peak-values. During the investigation it has been found that the bending moment for frequencies lower than the frequency where the peak occurs, is affected mostly by inertia. On the other side, for higher frequencies inertia seems to be relatively unimportant, the values here are dominated by hydrodynamic effects. It has previously been found that the linear seakeeping program tends to overpredict the motions at resonance for both heave and pitch, see Bingham et al. [3]. It is therefore no surprise that the load is overpredicted slightly at the same frequencies.

A transfer function for the bending moment with two maximum was also found by Lin et al. [16], when they investigated the bending moment on a series 60 hull. As can be seen from Figure 3-24 this is not found in the experiments, but according to Lin et al. it has been found in other experiments.

It has been stated earlier that non-linear effects are of great importance when calculating global loads. The possibility exists, that for the peak values, the non-linearities dominate, so that we will experience a higher value for the bending moment for a frequency higher than what is presented in Figure 3-24. Non-linearities means in this case non-linearities in the fluid problem, not in the structural problem. Since the deformations are assumed much smaller than the rigid-body motions, non-linearities in the fluid problem is more likely to show up. Lin et al. [16] did show that non-linearities contributed for $a/\lambda > 0.01$. λ is the wave-length and a the wave amplitude. This is in the regime of the experiments. The importance of non-linearities in the global loads is also documented by Kring et al. [14]. Non-linearities might be the

reason for the difference between the computational results and the experiments for extreme values.

Chapter 4

Multibody Interaction

In this chapter the generalized modes approach is used to study interaction problems. In these problems we have two or more bodies, and the motion of any one body is affected by the presence of the other bodies. In addition to the hydrodynamic interaction, physical constraints can be modeled in the same problem. An example where there are constraints between the bodies is the towing of a ship. Here, the physical constraint is represented by the towline. To carry out such a problem with generalized modes, we first solve for the hydrodynamic interaction in radiation and diffraction, then a simulation can be done where the constraints are incorporated properly into the equation of motion. A number of other problems fall into the category of interaction problems as well, such as different marine operations and transfer-at-sea problems. If we consider a replenishment operation where the constraints are very weak, we can idealize the problem by studying the hydrodynamic interaction only.

Consider two identical hulls separated by some finite distance in head seas. If we label the hulls A and B, B can be said to be the mirror of A, hence a wall is modeled in the middle of the gap. In the gap between the two ships waves will be present, and understanding these waves is important to predict the forces both at zero speed and forward speed. In a real replenishment operation it is not likely that the ships will be identical, but this is a straightforward extension of the example.

The configuration is shown in Figure 4-1. The separation is 1/2 L, where L is the ship-length, which means that the imaginary wall is located at half the distance

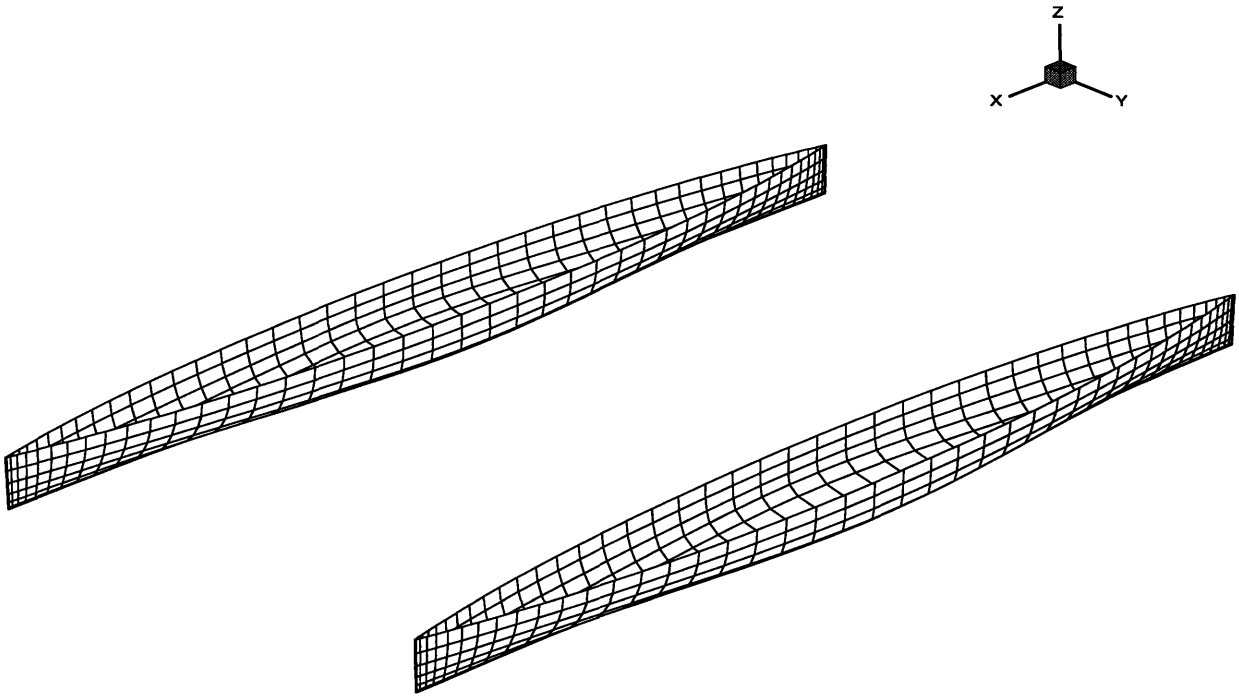

Figure 4-1: The configuration for the interaction problem with two Wigley hulls. The spacing is L/2 between the centers of the bodies.

between the bodies. This is a 12 degrees of freedom system, so we write the potential as

$$\Phi = \phi_I + \phi_S + \sum_{k=1}^{12} \phi_k \tag{4.1}$$

The role of generalized modes in this problem is to specify the boundary conditions(2.26) for these 12 modes. If we let potentials 1-6 represent the radiation potentials associated with body A, the boundary conditions for these potentials are homogeneous on body B, and vice versa for potentials 7-12. For instance for the surge modes 1 and 7

$$n_1 = \begin{cases} \bar{n}_1 & \mathbf{x} \in S_A \\ 0 & \mathbf{x} \in S_B \end{cases} \qquad n_7 = \begin{cases} 0 & \mathbf{x} \in S_A \\ \bar{n}_1 & \mathbf{x} \in S_B \end{cases} \tag{4.2}$$

where over-bar represent a vector component in the local frame. $\bar{n}_1$ is the normal vector in the x-direction, hence ϕ_1 and ϕ_7 are potentials associated with radiation in surge of body A and B respectively. The boundary conditions for the other modes are set up in the same way.

4.1 Zero Speed

First, results for zero speed in head seas are presented. Pitch and heave are of minor interest in such a problem, of more interest is the horizontal motions sway and yaw. In Figures 4-2 and 4-3 the diffraction impulse-response functions are presented, and the cross coupled radiation impulse-response functions are presented in Figures 4-4 and 4-5.

We see that the wave force on each of the two bodies have the same magnitude, but opposite signs. This is exactly what we would expect. The wave is reflected off the bodies, and is translating across the gap to hit the other body. Sway and yaw behave similarly. A similar reaction is also found in the radiation problem, except that the cross coupled radiation-impulse response functions are identical for the two hulls. Giving one body an impulsive velocity in one mode causes a force in the same mode on the other body after some finite time t, which is the time it takes the wave to move the distance between the bodies. This means that energy is trapped in the gap in some sense, only a minor part of the energy is radiated outwards each time the wave is reflected off the hull. The geometry of the ship is crucial for this radiation. If this problem were studied with another geometry, a barge for instance, the behavior would have been quantitatively different. With a barge close to a wall we would expect to see a even stronger trapping. Including forward speed for the Wigley hull should increase the energy loss in the gap. The magnitude of the response is larger in sway than in yaw, as can be predicted by the symmetry of the ship geometry.

4.2 Forward Speed

In this section results for two Wigley Hulls with spacing L/2 traveling in head seas at forward speed Fn=0.3 are presented. The geometry is identical to the problem investigated in the previous section, here we add forward speed effects.

In Figure 4-6 the diffraction impulse-response functions for the sway mode for the two ships are presented, the corresponding picture for yaw is presented in Figure 4-7.

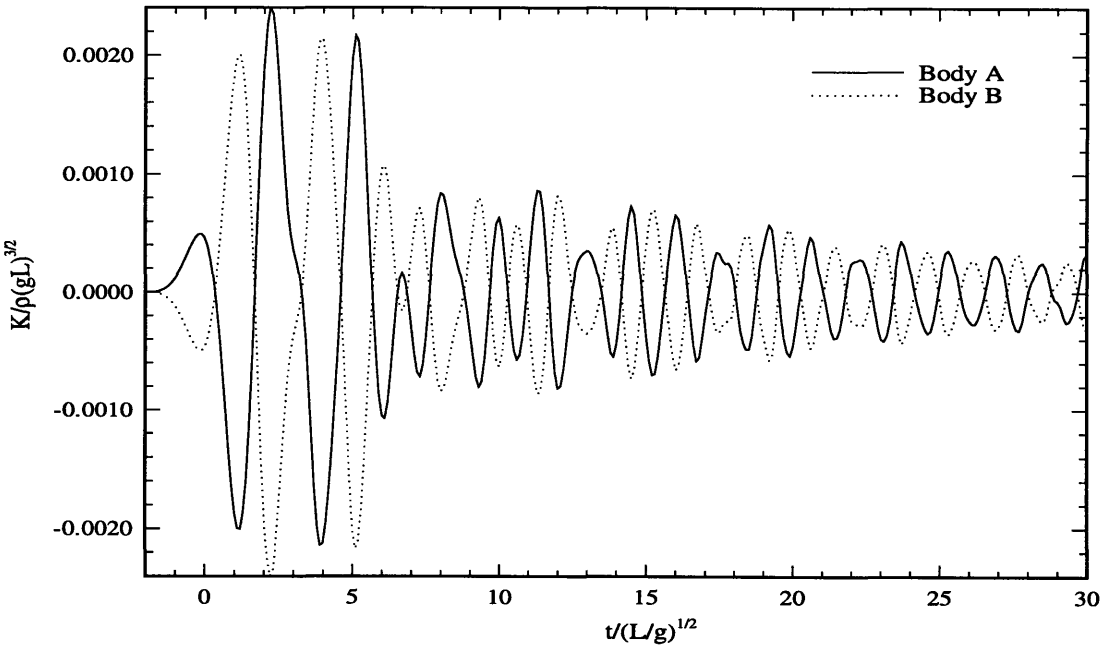

Figure 4-2: Diffraction impulse-response function, sway mode, for two Wigley hulls in head seas, Fn=0.0.

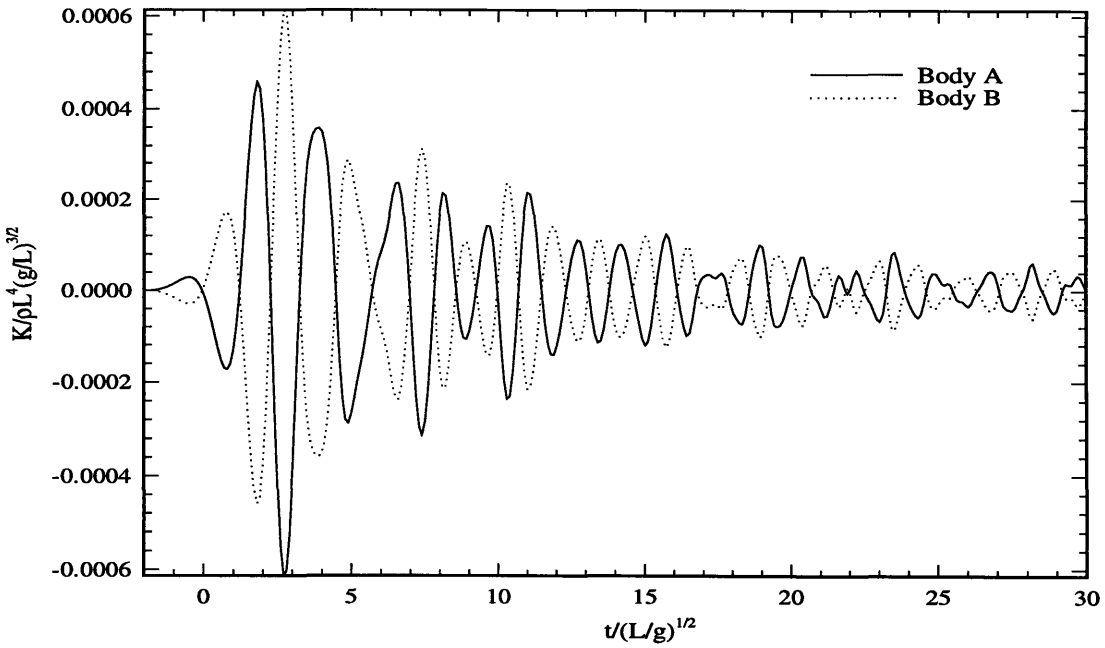

Figure 4-3: Diffraction impulse-response function, yaw mode, for two Wigley hulls in head seas, Fn=0.0.

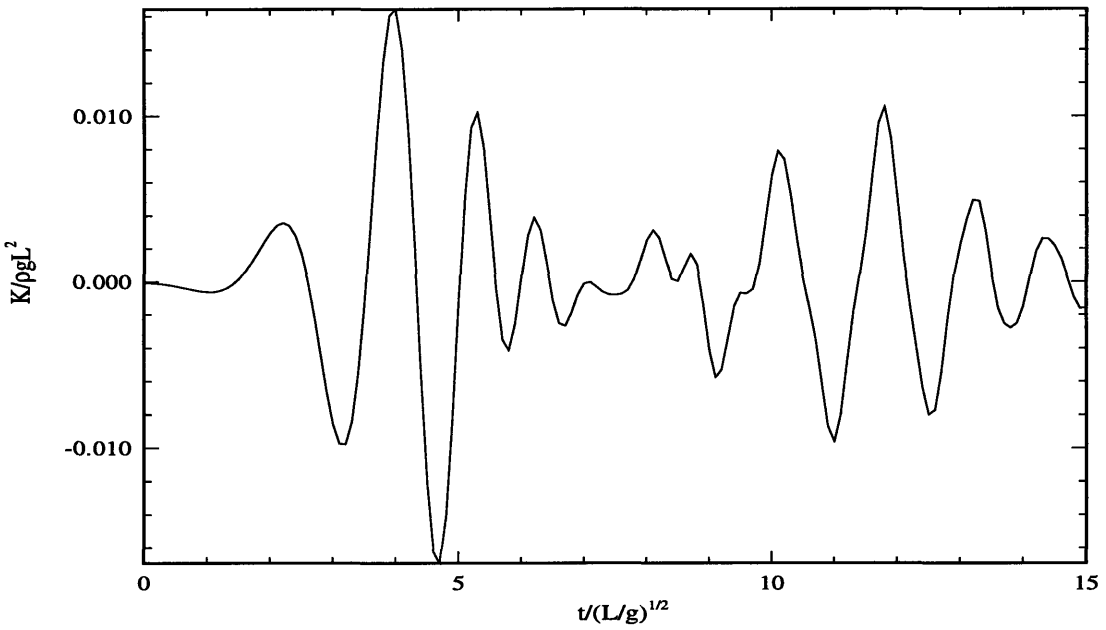

Figure 4-4: Radiation impulse-response function for two Wigley hulls in head seas, Fn=0.0. The graph shows the impulse-response in sway for body B due to an impulsive sway velocity of body A.

The difference from zero speed is immediately striking, the magnitude of the trapped wave is rapidly decaying to zero. As mentioned before, the energy loss in the gap is much larger when the ship is going forward, and after some time only specific waves can remain in the gap. Consider the group velocity of a wave as $\mathbf{v}_g = v_{gx}\mathbf{i} + v_{gy}\mathbf{j}$. Waves that can remain in the gap must have v_{gx} equal to the velocity of the ships, where as v_{gy} can be arbitrary. The component v_{gy} of the waves which are reflected must be a function of the ship geometry, so different geometries will lead to different patterns of the wave in the gap. The magnitude of the group velocity of the wave which can be found in Figure 4-6 is almost twice the velocity of the ships.

4.3 Steady Resistance

When two or more bodies are moving forward in proximity, it is very likely that the resistance will be changed from that of one body alone. Consider the formation

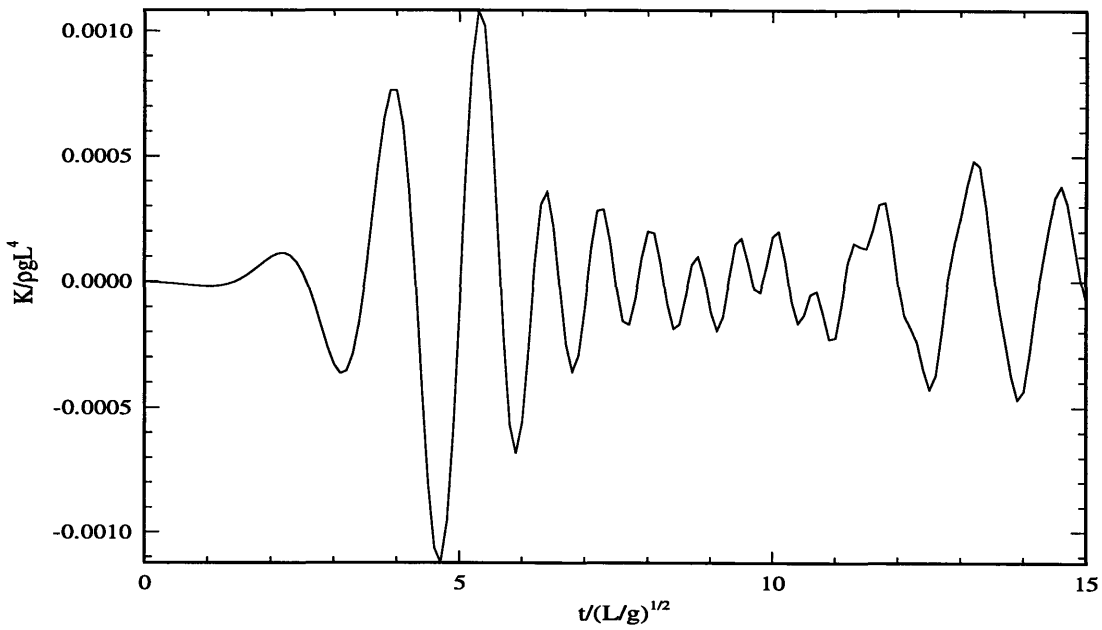

Figure 4-5: Radiation impulse-response function for two Wigley hulls in head seas, Fn=0.0. The graph shows the impulse-response in yaw for body A due to an impulsive yaw velocity of body B.

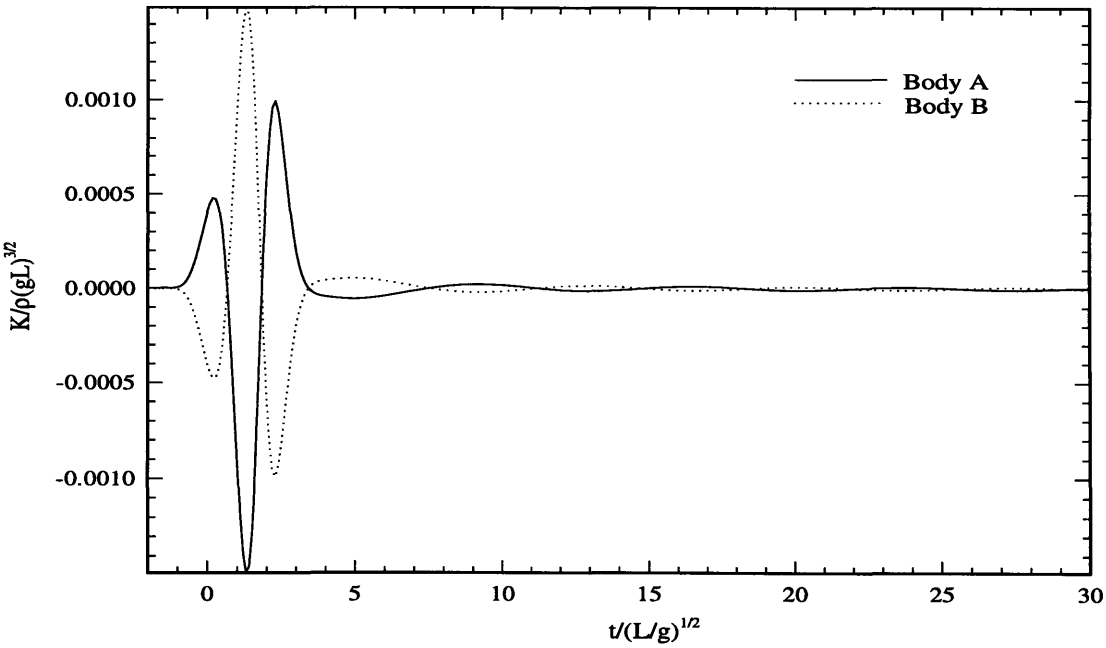

Figure 4-6: Diffraction impulse-response function, sway mode, for two Wigley hulls in head seas, Fn=0.3.

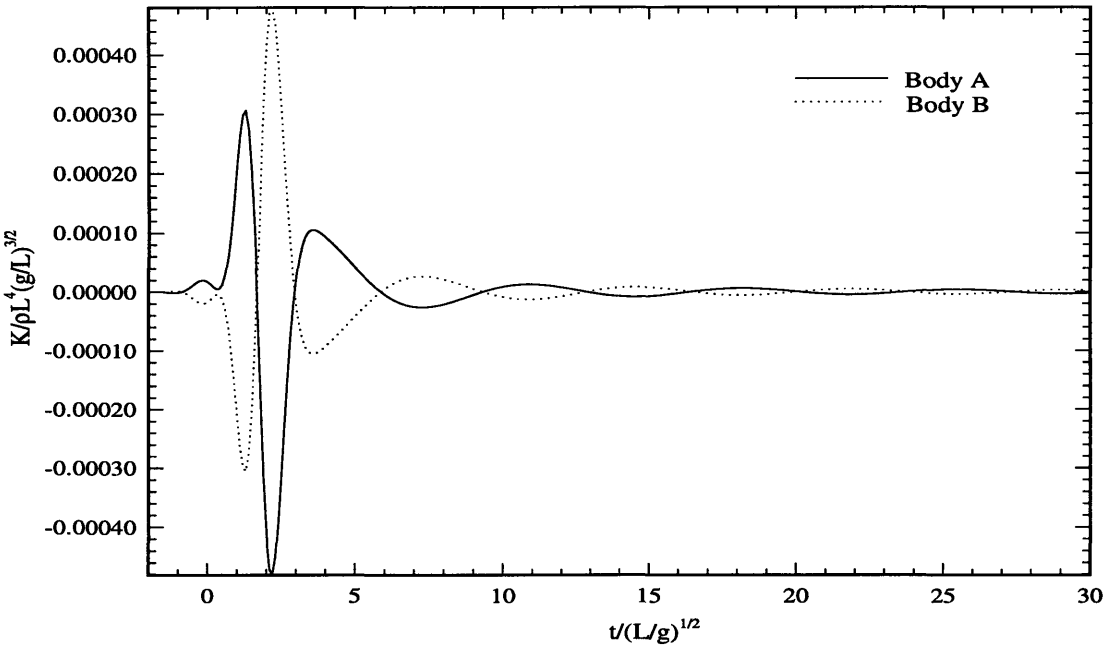

Figure 4-7: Diffraction impulse-response function, yaw mode, for two Wigley hulls in head seas, Fn=0.3.

a duck-family takes when it is swimming around in the pond. Can hydrodynamic interaction between the family members be the reason for such a formation? Is this arrow-shape formation optimum with respect to resistance? If that is the case, then there can be improved resistance in the formation of a convoy, for instance. If we consider a case where bodies are close together, it is obvious that wakes and waves from one body will affect another body, so resistance characteristics are of interest.

The approach taken here is to consider the wave resistance in such a problem. If we consider a 2D problem with two bodies traveling with forward speed, it can easily be shown that there is some optimum spacing which gives zero total resistance! If we let the separation distance between the two disturbances be l, this will happen if the spacing is some integer number of wavelengths, as explained by Newman [20]. It is therefore very likely that we can find something similar in 3D, even though we can not expect to find zero total resistance because of the radiation of energy.

In the previous case the aft body will get a 'free ride', it should however be noted

that in a problem with two submarines, the body in front can also get a 'free-ride' for some specific separations.

4.3.1 Formulation

The formulation of the steady pertubation potential $\bar{\phi}$ is given by Bingham et al. [3]. The potential can be calculated as the steady state limit of an impulsive acceleration to a forward speed U. The boundary conditions are given by

$$\left(\frac{\partial}{\partial t} - U\frac{\partial}{\partial x}\right)^2 \bar{\phi} + g\frac{\partial}{\partial z}\bar{\phi} = 0 \qquad \text{on } z = 0 \tag{4.3}$$

$$\phi_n = Un_1 h(t) \qquad \text{on } \bar{S}$$

$h(t)$ is the step-function, $h(t) = 0, t < 0, h(t) = 1, t \geq 0$.

To get the steady forces on the bodies we integrate the pressure force resulting from this potential over the bodies as $t \to \infty$. The force is

$$F_j = -\rho \int_{\bar{S}} \mathrm{dS} \left(\frac{\partial \bar{\phi}}{\partial t} - U\frac{\partial \bar{\phi}}{\partial x}\right) n_j \tag{4.4}$$

which in the steady state becomes

$$\bar{F}_j = \rho U \int_{\bar{S}} \mathrm{dS} \frac{\partial \bar{\phi}(x, t \to \infty)}{\partial x} n_j \tag{4.5}$$

Integration over each separate body will now result in a steady wave resistance.

4.3.2 Results

Results will be presented for two identical Wigley hulls with a spacing of two and three times the ship-length. The spacing is measured with respect to the center of each ship. Two different speeds have been used, both $Fn = 0.1$ and $Fn = 0.3$ have been investigated. Throughout this section the ship in front is labeled 'A', and the ship behind is labeled 'B'. The resistance of both ships are compared to that of a single ship alone.

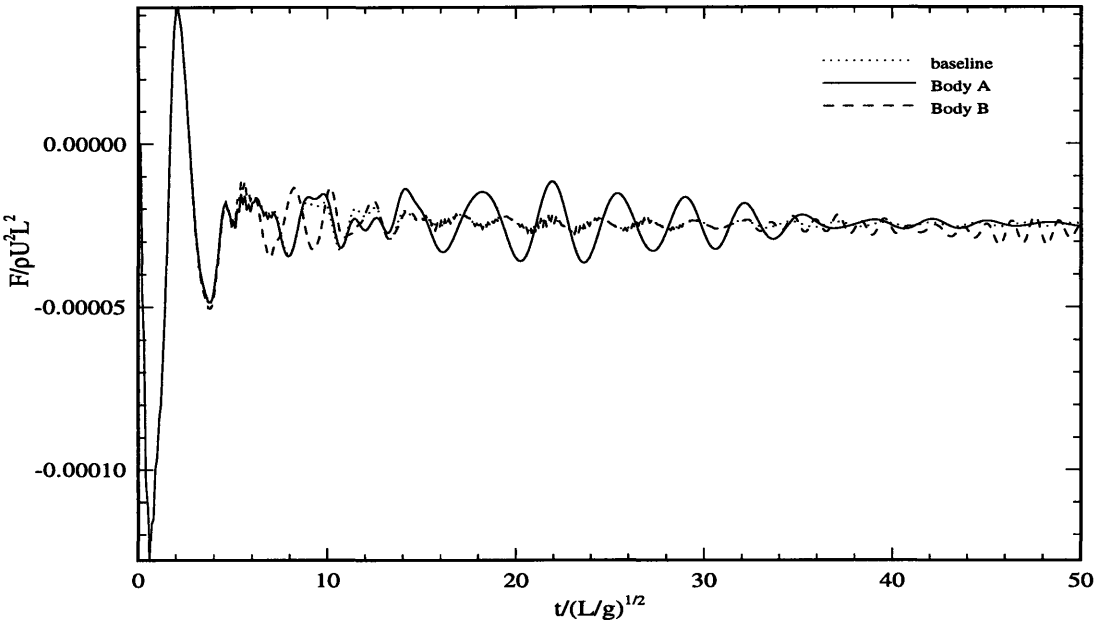

Figure 4-8: Steady resistance on two Wigley Hulls, separation of centers is 3 times the ship-length, Fn=0.1. Body A is the lead ship, body B is following A, where as the baseline is the single ship alone.

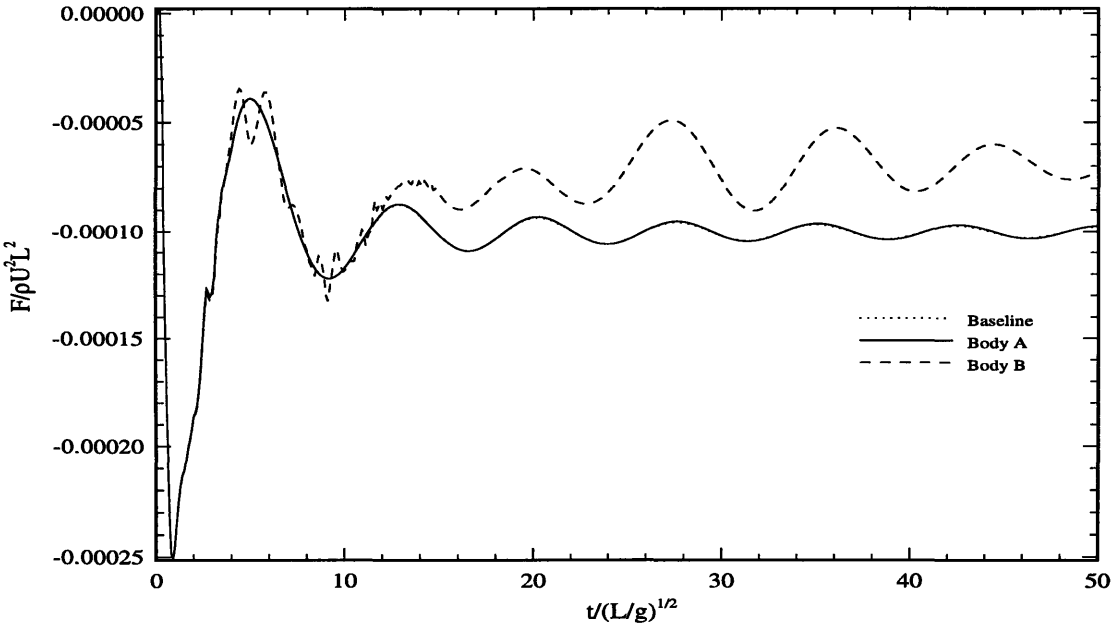

Figure 4-9: Steady resistance on two Wigley Hulls, separation of centers is 3 times the ship-length, Fn=0.3.

In Figures 4-8 and 4-9 the results for a separation distance of 3L are presented, $Fn = 0.1$ and $Fn = 0.3$, respectively. For low speed we find that there is no significant difference in the steady resistance, both ships have a resistance which compares well with the baseline of a single ship alone. For the higher speed of $Fn = 0.3$, this changes. The ship in front still has the same resistance as a single ship. However, the resistance on the ship behind is less. Note that the resistance is a negative quantity. The reduction in the wave resistance is about 25 percent. This is a significant reduction in resistance. In Figure 4-10 we have reduced the separation between the centers to two times the ship length. The resistance on body A is not affected by body B, but the resistance for body B is slightly larger than for body A. As can be seen from the graph, the resistance takes a very long time to become steady, so it is not possible from these results to state the increase in resistance exactly. Recalling the results which can be analytically obtained in 2D, the variation in resistance with velocity and separation distance makes sense. Bingham [2] show good agreement with experiments for a single ship, so this gives some confidence in the method used. It would therefore be very interesting to see experiments for two ships carried out for comparison with these results.

Using this approach to study interaction, the study of offshore towing can be improved. Milgram et al. [18] have studied towing and tow-line tension especially, using strip theory to calculate the hydrodynamic quantities. Two assumptions were used, the first that no hydrodynamic interaction was important, and secondly they used an ad-hoc procedure for the surge motion. Basing the hydrodynamic calculations on generalized modes theory, this can now be avoided. Interaction can be calculated, both cross-coupling in radiation and diffraction as well as wave-resistance can be found. These hydrodynamic quantities need only be calculated once, and combining them with an advanced towline model in a simulation routine, a towing simulation which takes into account the hydrodynamic interaction can be performed.

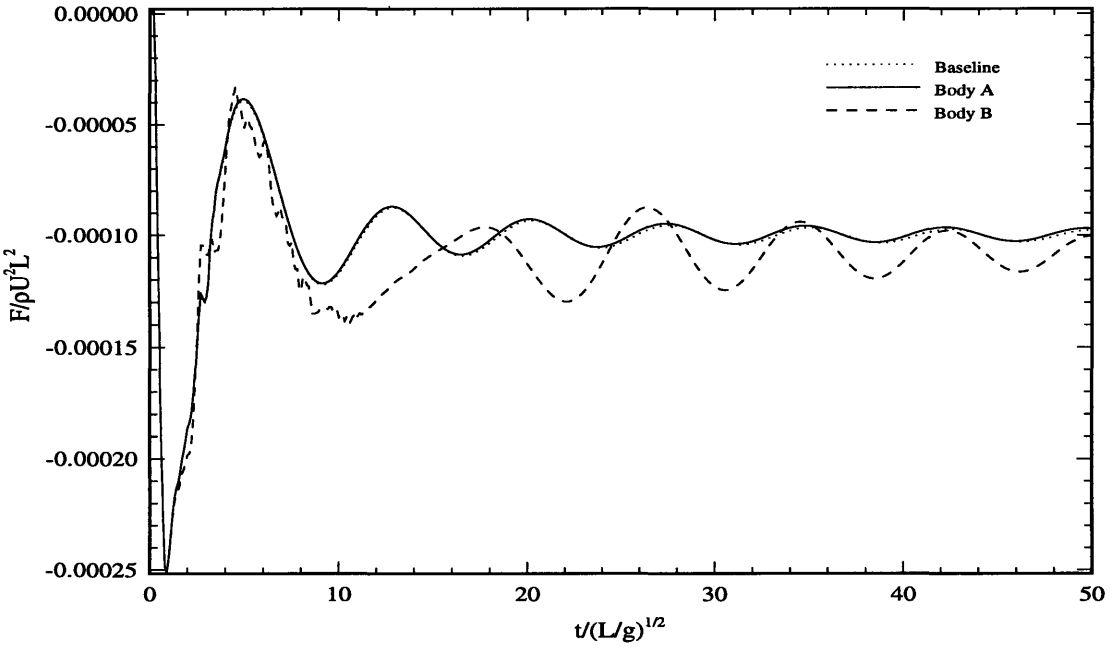

Figure 4-10: Steady resistance on two Wigley hulls, separation of centers is 2 times the ship-length, Fn=0.3.

Chapter 5

Conclusion

The linear transient seakeeping theory for 6 degrees of freedom has been reviewed and extended to N degrees of freedom, where forward speed effects are taken into account. Solving the problem is done using a free-surface Green function and a planar, constant strength, panel method.

Examples have been carried out for different types of problems and different types of modes. One group of problems fall into the category of hydroelastic problems, where structural properties are taken into account, and the equation of motion is solved for the N degree of freedom system. For a slender barge this has been done with both free-free beam modes and Legendre modes. It has been shown that the two sets of modes converge to the same result.

The method of generalized modes has also been used to calculate global loads in different structures, where radiation effects of the deformation are assumed negligible. In this case, the generalized modes theory can be used to efficiently expand the unknown force distribution in a set of chosen basis modes. Comparison between this method and the hydroelastic method have been done for a slender barge with intermediate stiffness, and the results are found to converge. Calculations have also been carried out for a Wigley hull, both at zero and forward speed. Comparison of the calculated bending moment at midship with experiments by Adegeest [1] has also been done, and good agreement was found for all wavelengths, except the wavelength which corresponds to the highest bending moment. It is believed that the non-linear

effects of the hydrodynamic problem are important for these wavelengths.

Generalized modes have also been used in interaction problems. Two different problems have been studied, the problem of two identical hulls side by side at zero or non-zero speed, and steady resistance of ships in proximity. In the problem where two hulls are separated transversely the behavior of the wave in the gap between the two bodies has been investigated. As could be expected, it has been demonstrated that waves seem to be trapped in the gap at zero speed, but this effect decreases rapidly as the bodies move forward.

Steady resistance calculations have been carried out for two ships traveling forward one ahead of the other, and it has been found that speed and distance between the ships gives very different resistance characteristics for the two bodies. Validation of the results is necessary to get confidence in the method.

Further research in this area would be to apply the method to a wide variety of problems, either involving fluid-structure problems, where the structural deformation is important for the hydrodynamic problem, or study global loads of structures which can be assumed stiff. Time-domain calculations of large volume structures like a mobile offshore base or a floating harbor/airport can also be done. The method should also be used to study the bending of a plate, where structural modes in two directions are utilized. This would especially be appropriate for a floating airport structure with wave directions not perpendicular to the structure. Modeling of the landing of an airplane is not possible in the frequency domain, if one wants to take this into account, time domain calculations are necessary.

More work should also be done in the validation of global loads. Good agreement with bending moment has been found, so it should be possible to get good results also for shear forces. Comparisons done so far has not given satisfactory results, and the results are therefore not included in this work.

For the interaction problems more work needs to be done to create algorithms that can simulate the interaction problems for all motions. In particular this would be of interest in the study of towing, where advanced tow-line models can be incorporated in the simulation routine. Other marine operations where several bodies interact

should also be investigated, especially if some kind of constraints are involved.

To increase the efficiency of the method, work has to be done on a more fundamental level, especially in terms of improving the computational speed of the method. Most of time used to solve the canonical problem is spent in the convolution over time (equation (B.14)), and methods to increase the speed of this calculation should be developed.

Appendix A

Describing the Normal Vector in the Mean Fixed Frame

Let the body boundary be described by the equation $g(x', y', z') = 0$. (x', y', z') are ship-fixed coordinates. A normal vector to this surface is $\mathbf{n}' = \nabla_{x'} g$ [9]. As the body may undergo unsteady, small motions about its mean position, this vector is to be described in a reference frame fixed to the mean position of the body. This coordinate system is denoted $\mathbf{x}$. The relationship between the systems is $\mathbf{x} = \mathbf{x}' + \boldsymbol{\alpha}(\mathbf{x}', t)$.

A normal vector in the $\mathbf{x}$-frame is now

$$\begin{aligned}
\mathbf{n} = \nabla g(x', y', z') &= \mathbf{i}\tfrac{\partial g}{\partial x} + \mathbf{j}\tfrac{\partial g}{\partial y} + \mathbf{k}\tfrac{\partial g}{\partial z} \\
&= \mathbf{i}[\tfrac{\partial g}{\partial x'}\tfrac{\partial x'}{\partial x} + \tfrac{\partial g}{\partial y'}\tfrac{\partial y'}{\partial x} + \tfrac{\partial g}{\partial z'}\tfrac{\partial z'}{\partial x}] \\
&= \mathbf{j}[\tfrac{\partial g}{\partial x'}\tfrac{\partial x'}{\partial y} + \tfrac{\partial g}{\partial y'}\tfrac{\partial y'}{\partial y} + \tfrac{\partial g}{\partial z'}\tfrac{\partial z'}{\partial y}] \\
&= \mathbf{k}[\tfrac{\partial g}{\partial x'}\tfrac{\partial x'}{\partial z} + \tfrac{\partial g}{\partial y'}\tfrac{\partial y'}{\partial z} + \tfrac{\partial g}{\partial z'}\tfrac{\partial z'}{\partial z}] \\
= \nabla_{x'} g - [\mathbf{i}\tfrac{\partial \boldsymbol{\alpha}}{\partial x} + \mathbf{j}\tfrac{\partial \boldsymbol{\alpha}}{\partial y} + \mathbf{k}\tfrac{\partial \boldsymbol{\alpha}}{\partial z}] \cdot \nabla_{x'} g \\
&= \mathbf{n}' - \nabla \boldsymbol{\alpha} \cdot \mathbf{n}'
\end{aligned} \tag{A.1}$$

Appendix B

An Integral Representation for the Canonical Potentials

B.1 Fixed frame of reference

Since all the potentials satisfy Laplace's equation in the fluid domain, and differ only in the body boundary conditions, the same procedure can be used to solve for all potentials. The Green function derived by Wehausen and Laitone [28] can be used to solve the problem efficiently:

$$G = (\mathbf{x};\boldsymbol{\xi},t) = G^{(0)}(\mathbf{x};\boldsymbol{\xi}) + G^{(f)}(\mathbf{x};\boldsymbol{\xi},t) \tag{B.1}$$

where

$$G^{(0)} = \left(\frac{1}{r} - \frac{1}{r'}\right) \qquad G^{(f)} = 2\int_0^\infty [1 - cos\sqrt{gkt}]e^{(z+\zeta)}J_0(kR)dk$$

$$\left.\begin{matrix} r \\ r' \end{matrix}\right\} = \sqrt{(x-\xi)^2 + (y-\eta)^2 + (z \mp \zeta)^2} \tag{B.2}$$

$$R = \sqrt{(x-\xi)^2 + (y-\eta)^2}$$

J_0 is the Bessel function of zero order. Green's second identity states that

$$\int_{\nu}[\varphi\nabla^2 G - G\nabla^2\varphi]d\boldsymbol{\xi} = \int_{S}[\varphi G_n - G\varphi_n]d\boldsymbol{\xi} = 0 \tag{B.3}$$

where the surface S is a sum of the surface of the body, the free surface, infinity and S_ϵ which is a small neighborhood around the singular point of $G^{(0)}$. Applying Green's second identity to φ_τ and G and using that the integration in infinity goes to zero [11], we get

$$2\pi\varphi_\tau + \int_{S_b}[\varphi_\tau G_n - \varphi_{\tau n}G]d\boldsymbol{\xi} + \int_{S_f}[\varphi_\tau G_n - \varphi_{\tau n}G]d\boldsymbol{\xi} = 0 \tag{B.4}$$

ϕ_t is the time derivative of the potential. S_b denotes the body boundary and S_f the free surface. Integrating over time from $-\infty$ to t we get

$$\begin{aligned} &2\pi\varphi(t) + \textstyle\int_{S_b}[\varphi(t)G_n(0) - G(0)\varphi_n]d\boldsymbol{\xi} - \int_{-\infty}^{t}(\int_{S_b}[\varphi G_{\tau n} - \varphi_n G_\tau]d\boldsymbol{\xi})d\tau \\ &+ \textstyle\int_{S_f}[\varphi(t)G_n(0) - \varphi_n(t)G(0)]d\boldsymbol{\xi} - \int_{-\infty}^{t}(\int_{S_f}[\varphi G_{\tau n} - \varphi_n G_\tau]d\boldsymbol{\xi})d\tau = 0 \end{aligned} \tag{B.5}$$

At this point, we can invoke the free surface condition for G. In a fixed frame of reference we can use (2.11) and recalling that the normal vector to the plane $z = 0$ is $\mathbf{k}$, we write

$$\frac{\partial}{\partial z} = \mathbf{n}\cdot\nabla = -\frac{1}{g}\frac{\partial^2}{\partial t^2} \qquad z = 0 \tag{B.6}$$

Evaluating the last term in (B.5), this is written

$$I = -\int_{-\infty}^{t}(\int_{S_f}[\varphi G_{\tau n} - \varphi_n G_\tau]d\boldsymbol{\xi})d\tau = -\frac{1}{g}\int_{-\infty}^{t}(\int_{S_f}\frac{\partial}{\partial\tau}[\varphi G_{\tau\tau} - \varphi_\tau G_\tau]d\boldsymbol{\xi})d\tau \tag{B.7}$$

In 2D the transport theorem takes the form

$$\frac{d}{dt}\int_{S_f(t)} f d\boldsymbol{\xi} = \int_{S_f(t)}\frac{\partial}{\partial t}f d\boldsymbol{\xi} + \int_{C(t)} f\mathbf{U}\cdot\mathbf{n}dl \tag{B.8}$$

when S_f moves with the speed $\mathbf{U}$. The contour $C(t) = \Gamma(t) + C_\infty$, Γ is the waterline

of the moving body. Applying this theorem to (B.7), we write

$$I = -\int_{S_f} \varphi(t) G_n(0) d\boldsymbol{\xi} - \frac{1}{g}\int_{-\infty}^{t} (\int_{\Gamma} [\varphi G_{\tau\tau} - \varphi_\tau G_\tau] n_1 dl) d\tau \tag{B.9}$$

Substituting back into (B.5), using initial and boundary conditions, we get an earth fixed integral equation for the unknown potential φ.

$$\begin{array}{c} 2\pi\varphi(t) + \int_{S_b}[\varphi(t)G_n(0) - G(0)\varphi_n]d\boldsymbol{\xi} - \int_{-\infty}^{t}(\int_{S_b}[\varphi G_{\tau n} - \varphi_n G_\tau]d\boldsymbol{\xi})d\tau \\ -\frac{U}{g}\int_{-\infty}^{t}(\int_{\Gamma}[\varphi G_{\tau\tau} - \varphi_\tau G_\tau]n_1 dl)d\tau = 0 \end{array} \tag{B.10}$$

B.2 Steady translating coordinate system

We are about to solve the linearized boundary value problem in a coordinate system moving with steady forward speed, attached to a mean position of the moving body. Recall that a time derivative of a function in the fixed coordinate system is equivalent to a substantial derivative in the moving frame of reference, so we get the relations

$$x_0 = x + Ut \qquad \frac{\partial}{\partial t} \rightarrow \frac{\partial}{\partial t} - U\frac{\partial}{\partial x} \tag{B.11}$$

This means that the Green function has a different form, the parameter R is

$$R = \sqrt{(x - \xi + Ut)^2 + (y - \eta)^2}$$

With this change in the Green function, the function satisfies the free-surface boundary condition in the steady moving frame. The integral equation (B.10) now takes the form

$$\begin{array}{c} 2\pi\varphi(t) + \int_{S_b}[\varphi(t)G_n(0) - G(0)\varphi_n]d\boldsymbol{\xi} - \int_{-\infty}^{t}(\int_{S_b}[\varphi G_{\tau n} - \varphi_n G_\tau]d\boldsymbol{\xi})d\tau \\ -\frac{U}{g}\int_{-\infty}^{t}(\int_{\Gamma} n_1[\varphi(G_{\tau\tau} - UG_{\tau\xi}) - G_\tau(\varphi_\tau - U\varphi_\xi)]dl)d\tau \\ = U\int_{-\infty}^{t}(\int_{S_b}[\varphi G_{\xi n} + \varphi_n G_\xi]d\boldsymbol{\xi})d\tau \\ +\frac{U^2}{g}\int_{-\infty}^{t}(\int_{\Gamma} n_1[G_\xi(\varphi_\tau - U\varphi_\xi) - \varphi(G_{\tau\xi} - UG_{\xi\xi})]dl)d\tau \end{array} \tag{B.12}$$

It has been shown [2] that the waterline integral on the right hand side of (B.12) can be written

$$\frac{1}{g}\int_{\Gamma} d\eta[G_{\xi}(\varphi_{\tau}-U\varphi_{\xi})-\varphi(G_{\xi\tau}-UG_{\xi\xi})]=\int_{S_f} d\boldsymbol{\xi}[\varphi G_{\xi n}-G_{\xi}\varphi_n] \tag{B.13}$$

where the integration is carried out in a counter clockwise direction, so $n_1 dl = -d\eta$. Recall that G_{ξ} is a harmonic function and apply Green's second identity to the right hand side of (B.12), the expression vanishes. The forward speed, integral equation for the canonical potential φ then can be expressed as

$$\begin{aligned} &2\pi\varphi(t)+\int_{S_b}[\varphi(t)G_n(0)-G(0)\varphi_n]d\boldsymbol{\xi}-\int_{-\infty}^{t}(\int_{S_b}[\varphi G_{\tau n}-\varphi_n G_{\tau}]d\boldsymbol{\xi})d\tau \\ &-\tfrac{U}{g}\int_{-\infty}^{t}(\int_{\Gamma} n_1[\varphi(G_{\tau\tau}-UG_{\tau\xi})-G_{\tau}(\varphi_{\tau}-U\varphi_{\xi})]dl)d\tau=0 \end{aligned} \tag{B.14}$$

The Neumann boundary conditions for the potentials are known from Section (2.2).

Appendix C

Forces Evaluated Using Tuck's Theorem

Recall Tuck's Theorem [24]:

$$\int_{\bar{S}}[m_j\Phi_k - n_j(\nabla\bar{\varphi}\cdot\nabla\Phi_k)]dS = -\int_{\bar{\Gamma}} n_j\Phi_k(\mathbf{l}\times\mathbf{n})\cdot\nabla\bar{\varphi} \tag{C.1}$$

$\mathbf{l}$ is the unit tangent vector to the mean waterline. The theorem is most useful if the body is wall sided along the waterline, since the term on the right hand side of (C.1) vanishes. We will assume that this is the case, and write (2.63) as

$$F_{jk} = -\rho\int_{\bar{S}}(\frac{\partial\Phi_k}{\partial t}n_j - \Phi_k m_j)dS \tag{C.2}$$

The force due to the radiation pressure now becomes

$$\begin{array}{c} F_{jk} = -\rho\int_{\bar{S}}[(\mathcal{N}_k\ddot{x}_k + \mathcal{M}_k\dot{x}_k + \int_{-\infty}^{t}\frac{\partial\psi_k}{\partial t}(t-\tau)\dot{x}_k(\tau)d\tau)n_j \\ -(\mathcal{N}_k\dot{x}_k + \mathcal{M}_k x_k + \int_{-\infty}^{t}\psi_k(t-\tau)\dot{x}_k(\tau)d\tau)m_j]dS \end{array} \tag{C.3}$$

Bibliography

[1] Adegeest, L. J. M., "Experimental investigation of the influence of bow flare and forward speed on the non linear vertical motions, bending moments and shear forces in extreme regular wave conditions.", Technical Report 993, Delft University of Technology, The Netherlands, 1994.

[2] Bingham, H. B., "Simulating Ship Motions in the Time Domain." Ph.D. thesis, Department of Ocean Engineering, MIT, February 1994.

[3] Bingham, H. B., Korsmeyer, F. T., Newman, J, N., Osborne, G. E., "The Simulation of Ship Motions", *6th International Conference on Numerical Ship Hydrodynamics*, 1993.

[4] Bingham, H. B., Korsmeyer. F. T., Newman, J. N., "Prediction of the Seakeeping Charateristics of Ships", *20th Symposium on Naval Hydrodynamics*, 1994.

[5] Bishop, R. E. D, Price, W. G., *Hydroelasticity of Ships*, Cambridge University Press, Cambridge, 1979.

[6] Bishop, R. E. D., Price, W. G., Wu, Y., "A general linear hydroelastic theory of floating structures moving in a seaway", *Phil. Trans. R. Soc. London*, **A 316**, pp.374–426, 1986.

[7] Gran, S., *A Course in Ocean Engineering*, Elsevier Science Publishers B.V., 1992.

[8] Hermundstad, O. A., Wu, M., Moan, T., "Hydroelastic response analysis of a high speed monohull", in Faltinsen O., et al. (eds) *Hydroelasticiy in Marine Technology*, Balkema, Rotterdam, 1994.

[9] Hildebrand, F. B., *Advanced Calculus for Applications.*, Prentice–Hall, Inc., 1976.

[10] Kashiwagi, M., "A Precise Calculation Method for Hydroelastic Behaviors of Very Large Floating Structures", *11th Workshop on Water Waves and Floating Bodies*, 1996.

[11] Korsmeyer, F. T., Bingham H. B., Newman, J. N., "The forward speed diffraction problem". In preparation.

[12] Korsmeyer, F. T., Bingham, H. B., Newman, J. N., *TĪMIT 2.1*, A panel-method program for transient wave-body interactions. The Department of Ocean Engineering, Massachusetts Institute of Technology.

[13] Korsmeyer, F. T., Lee., C.-H., Newman, J.N., Sclavounos, P.D., "The Analysis of Wave Effects on Tension-Leg Platforms", *Seventh International Conference on Offshore Mechanics and Arcitc Engineering*, 1988.

[14] Kring, D., Huang, Y.-F., Sclavounos, P., Vada, T., Braaten, A., "Nonlinear Ship Motions and Wave-Induced Loads by a Rankine Method", *21st Symposium on Naval Hydrodynamics*, 1996.

[15] Lee, C.-H., "WAMIT Theory Manual", Report 95-2, 1995, The Department of Ocean Engineering, Massachusetts Institute of Technology.

[16] Lin, W.-M., Meinhold, M., Salvesen, N., Yue, D., "Large-Amplitude Motions and Wave Loads for Ship Design", *20th Symposium on Naval Hydrodynamics*, 1994.

[17] Maniar, H. D., Newman, J, N., "Wave Diffraction by a Long Array of Cylinders", submitted to the *Journal of Fluid Mechanics.*

[18] Milgram, J. H., Triantafyllou, M. S., Frimm, F. C., Anagnostou, G., "Seakeeping and Extreme Tensions in Offshore Towing", *SNAME Transactions*, Vol. 96, 1988.

[19] Newman, J. N., "Wave Effects on Deformable Bodies", *Applied Ocean Research*, **16**, pp. 47-59, 1994.

[20] Newman, J. N., *Marine Hydrodynamics*, The MIT Press, Cambridge, Massachusetts, 1977.

[21] Newman, J. N., "The theory of ship motions",*Advances in Applied Mechanics*, Vol. 18, pp.222–283, 1978.

[22] Newman J. N., Sclavounos, P. D., "The Computation of Wave Loads on Large Offshore Structures", *BOSS Conference 1988.*

[23] Newman, J. N., Maniar, H. D., Lee, C.-H., "Analysis of Wave Effects for Very Large Floating Structures", *International Workshop on Very Large Floating Structures, VLFS'96*, 1996.

[24] Oglivie, T. F., Tuck, E. O., " A Rational Strip Theory for Ship Motions, part 1". Techincal Report 013, The Department of Naval Architecture and Marine Engineering, The Univeristy of Michigan, Ann Arbor, Michigan, 1969.

[25] Paulling, J. R., "Strength of Ships", in Lewis, E. V. (ed.) *Principles of Naval Architecture*, Vol.1, 1988.

[26] Strauss, W. A., *Partial Differential Equations*, John Wiley & Sons, Inc., 1992.

[27] Timman, R., Newman, J.N., "The Coupled Damping Coefficients of a Symmetric Ship", *Journal of Ship Research*, Vol 5, 1962

[28] Wehausen, J.V. and Laitone, E.V., "Surface waves", *Handbuch der Physik*, **9**, pp. 446–778, Springer, 1960.

[29] Wu, C., Watanabe, E., Utsunomiya, T., "An Eigenfunction Expansion-Matching for Analyzing the Wave-Induced Responses of an Elastic Floating Plate", *Applied Ocean Research*, Vol 17, 1995.

[30] Wu, M., Moan, T., "Linear and Nonlinear Hydroelastic Analysis of High-Speed Vessels", *Journal of Ship Research*, Vol 40, No2, 1996.